

# Chameleon: Episodic Memory for Long-Horizon Robotic Manipulation

Xinying Guo<sup>1,2,\*</sup>, Chenxi Jiang<sup>1,\*</sup>, Hyun Bin Kim<sup>1</sup>, Ying Sun<sup>2</sup>, Yang Xiao<sup>1</sup>, Yuhang Han<sup>3</sup>, Jianfei Yang<sup>1,†</sup>

<sup>1</sup>MARS Lab, Nanyang Technological University, <sup>2</sup>Institute for Infocomm Research, A\*STAR, Singapore, <sup>3</sup>National University of Singapore

\*Equal Contribution, †Corresponding Author

Robotic manipulation often requires memory: occlusion and state changes can make decision-time observations perceptually aliased, making action selection non-Markovian at the observation level because the same observation may arise from different interaction histories. Most embodied agents implement memory via semantically compressed traces and similarity-based retrieval, which discards disambiguating fine-grained perceptual cues and can return perceptually similar but decision-irrelevant episodes. Inspired by human episodic memory, we propose **Chameleon**, which writes geometry-grounded multimodal tokens to preserve disambiguating context and produces goal-directed recall through a differentiable memory stack. We also introduce **Camo-Dataset**, a real-robot UR5e dataset spanning episodic recall, spatial tracking, and sequential manipulation under perceptual aliasing. Across tasks, Chameleon consistently improves decision reliability and long-horizon control over strong baselines in perceptually confusable settings.

**Correspondence:** Jianfei Yang at [jianfei.yang@ntu.edu.sg](mailto:jianfei.yang@ntu.edu.sg)

**Code:** [https://github.com/gxyes/MARS\\_Chameleon](https://github.com/gxyes/MARS_Chameleon)



## 1 Introduction

Robotic manipulation in the real world often requires acting from memory. As manipulation unfolds, task-relevant state can become occluded or overwritten, making the decision point non-Markovian at the observation level and forcing correct actions to depend on historical interactions. This makes long-horizon memory a central bottleneck for embodied intelligence. Figure 1 illustrates the challenge in the shell game: when identical cups become indistinguishable at grasp time, the robot must rely on swap history to select the correct cup.

A common solution is to equip an agent with long-term memory that is written during interaction and used later. In many embodied systems, this memory is language-centric: experience is summarized into semantically compressed, text-like traces, mirroring retrieval-augmented generation (RAG) popularized by large language models (LLMs) Lewis et al. (2020). Such compression is ill-suited to perceptual aliasing in robotic memory-intensive tasks, because it removes disambiguating perceptual context that determines the correct action, including spatial relations, viewpoint-dependent evidence, and the outcomes of prior interactions Wang et al. (2025); Liu et al. (2024);

Fung et al. (2025). In Figure 1, a summary such as “the ball is under a cup” can be semantically correct yet still insufficient to identify the correct cup after swaps. Recent work, therefore, augments embodied agents with visual history buffers Lin et al. (2025), but similarity-driven access still induces interference when repeated, similar scenes correspond to different histories. Together, these limitations expose failures at both writing and retrieval: memory must be written as disambiguated, indexable events to reduce interference, and retrieved based on whether it supports the current goal and near-future outcome, rather than on similarity.

Biological episodic memory implements precisely these two functions. In evolutionary accounts, episodic memory is often viewed as a foundation of intelligence that predates abstract, symbolic reasoning Allen and Fortin (2013); it organizes experience as events bound to spatiotemporal and causal context, enabling prospective behavior even without language. Non-linguistic animals provide concrete evidence of event-based planning, such as food-caching birds that remember what was stored, where it was stored, and when it was stored, and use these memories to guide later retrieval decisions Worsfold et al. (2025). Mechanistically, episodic memory is commonly attributed

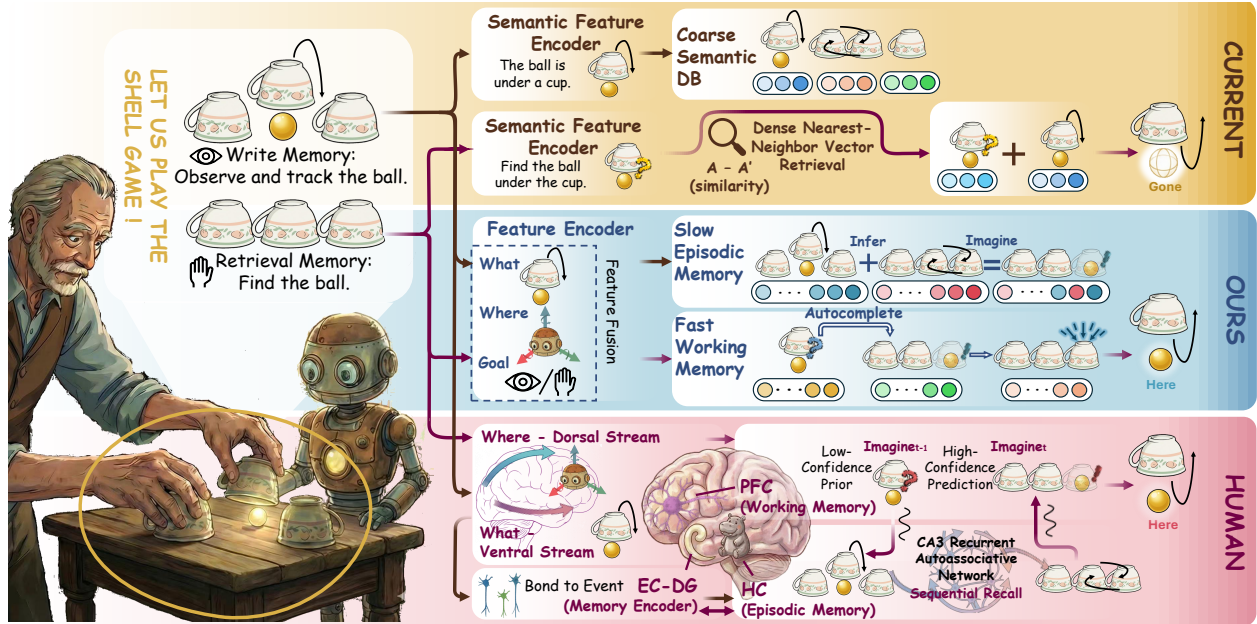


**Figure 1 Memory-intensive robotic manipulation is often perceptually aliased:** in the shell game, identical cups look the same at decision time while the correct grasp depends on earlier interactions. Existing approaches often discard fine-grained details needed for reliable decision-making. Inspired by the human Entorhinal Cortex–Hippocampus–Prefrontal Cortex (EC–HC–PFC) episodic memory system, we propose Chameleon for episodic recall, spatial tracking, and long-horizon task completion.

to coordinated dynamics across the entorhinal cortex (EC), hippocampal formation (HC), and prefrontal cortex (PFC) Bakker et al. (2008); Zheng et al. (2025). Within HC, the dentate gyrus (DG) supports pattern separation, reducing interference so similar experiences are stored as distinct traces Bakker et al. (2008); CA3 supports pattern completion via associative retrieval from partial cues; and CA1 supports episodic representations that bind recalled content into a contextualized event for downstream use. PFC control biases recall toward memories that are relevant to current goals and anticipated near-future outcomes, rather than by similarity alone Zheng et al. (2025). Viewed through this lens, perceptual aliasing exposes two algorithmic gaps in current embodied systems: how to form disambiguated, indexable event representations during memory formation, and how to learn goal-directed retrieval so recall is driven by decision utility.

To address these gaps, we propose Chameleon, a bio-inspired memory architecture for long-horizon embodied manipulation. A geometry-grounded perception module converts multi-view observations into view-consistent patch tokens anchored to the end-effector, preserving evidence needed for disambiguation at write time. A hierarchical differentiable memory stack couples an episodic state with a working state through continuous dynamics and produces a

compact decision state. HoloHead shapes this state with a latent imagination objective that trains the decision state to be predictive of near-future state evolution. Conditioned only on the resulting state, a rectified-flow policy generates an end-effector pose trajectory in one shot, improving stability for long-horizon control.

To systematically evaluate our proposed Chameleon, we introduce Camo-Dataset, a real-world dataset collected on a physical UR5e robot. It comprises episodic recall, spatial tracking, and sequential manipulation tasks designed to enforce perceptual aliasing while requiring history-dependent decisions. We compare Chameleon against strong baselines, including Diffusion Policy Chi et al. (2023), Flow Matching Zhang and Gienger (2024), and ACT Zhao et al. (2023), and against five ablated variants under identical conditions. Across metrics including success rate, decision success rate, and manipulation success rate, Chameleon consistently improves decision reliability and long-horizon task completion. We also probe the learned memory state and observe separation between perceptually similar yet memory-distinct states, as well as pattern completion behavior enabled by the HoloHead objective.

Our contributions are threefold:

- (1) **Perceptual Aliasing Problem Formulation:** We for-

mulate robotic memory-intensive tasks as decision problems with perceptual aliasing, where similar decision-time observations can require different actions conditioned on interaction history, highlighting the need for episodic memory.

(2) **Bio-inspired Hierarchical Episodic Memory Architecture:** We propose Chameleon, a bio-inspired hierarchical memory architecture that integrates geometry-grounded disambiguating encoding, differentiable goal-directed retrieval trained via HoloHead, and memory-conditioned rectified-flow control for long-horizon manipulation.

(3) **Real-robot Episodic Memory Dataset and Analysis:** We introduce Camo-Dataset, a UR5e real-robot dataset for episodic recall, spatial tracking, and sequential manipulation under perceptual aliasing, together with quantitative evaluation and representation-level analyses.

## 2 Related Works

With advances in neuroscience, memory is commonly categorized into non-declarative and declarative memory [Squire \(1992\)](#). Non-declarative memory is expressed through behavioral performance, including skills and habits, whereas declarative memory involves conscious recall of facts and events. Within declarative memory, episodic memory is supported by pattern separation and pattern completion [Bakker et al. \(2008\)](#). Pattern separation integrates multimodal sensory streams into distinct event representations to disambiguate similar perceptions, while pattern completion retrieves events from partial cues to support downstream decisions [Dickerson and Eichenbaum \(2010\)](#); [Ngo et al. \(2021\)](#); [Amer and Davachi \(2023\)](#).

In artificial intelligence, memory is often divided into parametric and non-parametric memory (analogous to knowledge and episodic memory, respectively) [Mallen et al. \(2023\)](#); [Su et al. \(2025\)](#); [Teyler and DiScenna \(1986\)](#). Parametric memory encodes cross-task knowledge within model parameters, while non-parametric mechanisms store task-specific context. Many LLM-based agents adopt retrieval-augmented generation (RAG), querying external knowledge repositories via embedding-based similarity search to simulate long-term memory [Lewis et al. \(2020\)](#); [Karpukhin et al. \(2020\)](#); [Borgeaud et al. \(2022\)](#); [Yao et al. \(2022\)](#); [Park et al. \(2023\)](#). However, retrieval remains challenging in zero-shot settings due to the lack of relevance supervision [Gao et al. \(2023\)](#), and semantic similarity does not necessarily correspond to task utility [Fang et al. \(2024\)](#).

Therefore, recent work augments retrieval with structured knowledge or query transformation to better capture long-range dependencies and reduce semantic gaps [Wan et al. \(2025\)](#); [Jimenez Gutierrez et al. \(2024\)](#); [Gao et al. \(2023\)](#).

In embodied intelligence, memory mechanisms are often inherited from LLM paradigms, relying on semantic embeddings or sparse topological maps to encode object relations and spatial structure [Xie et al. \(2024\)](#); [Zhu et al. \(2024\)](#); [Mon-Williams et al. \(2025\)](#); [Anwar et al. \(2025\)](#). Such abstractions compress continuous physical states into symbolic representations and discard fine-grained dynamics [Liu et al. \(2025\)](#); [Fang et al. \(2026\)](#). However, manipulation in unstructured environments requires tracking object poses, surface properties, contact dynamics, and evolving state transitions. This mismatch between semantic memory and physical dynamics limits the generalization and operational accuracy of VLA systems.

## 3 Method

### 3.1 Overview

*Motivation.* Robotic memory-intensive tasks often arise under perceptual aliasing: similar sensory inputs can require different decisions because the disambiguating context is occluded, transient, or established only through earlier interactions. Human episodic memory addresses this failure mode by combining disambiguating encoding, goal-directed recall, and a working state that supports online control. Motivated by the functional roles of the EC–HC–PFC system, Chameleon implements these requirements in a fully differentiable architecture with a single decision state used as input to the policy.

*Problem setup.* At each timestep  $t$ , the agent receives a multimodal observation  $o_t = \{I_t^f, I_t^h, s_t, \psi_t\}$ , where  $I_t^f$  and  $I_t^h$  are RGB images from a fixed front camera and a hand-mounted side camera,  $s_t$  denotes the robot proprioceptive state including end-effector pose and gripper state, and  $\psi_t$  is an optional task-phase indicator (e.g., a discrete 0/1 signal denoting an observe phase versus an act phase) that specifies the interaction mode rather than revealing the hidden task state. Rather than predicting a single-step command, we parameterize control by generating a future end-effector (EE) pose trajectory over a horizon  $H$  (Section 3.4). During training, we supervise the model with ground-truth future pose trajectories  $x_{t:t+H} \in \mathbb{R}^{H \times d_{\text{raw}}}$ . During inference,

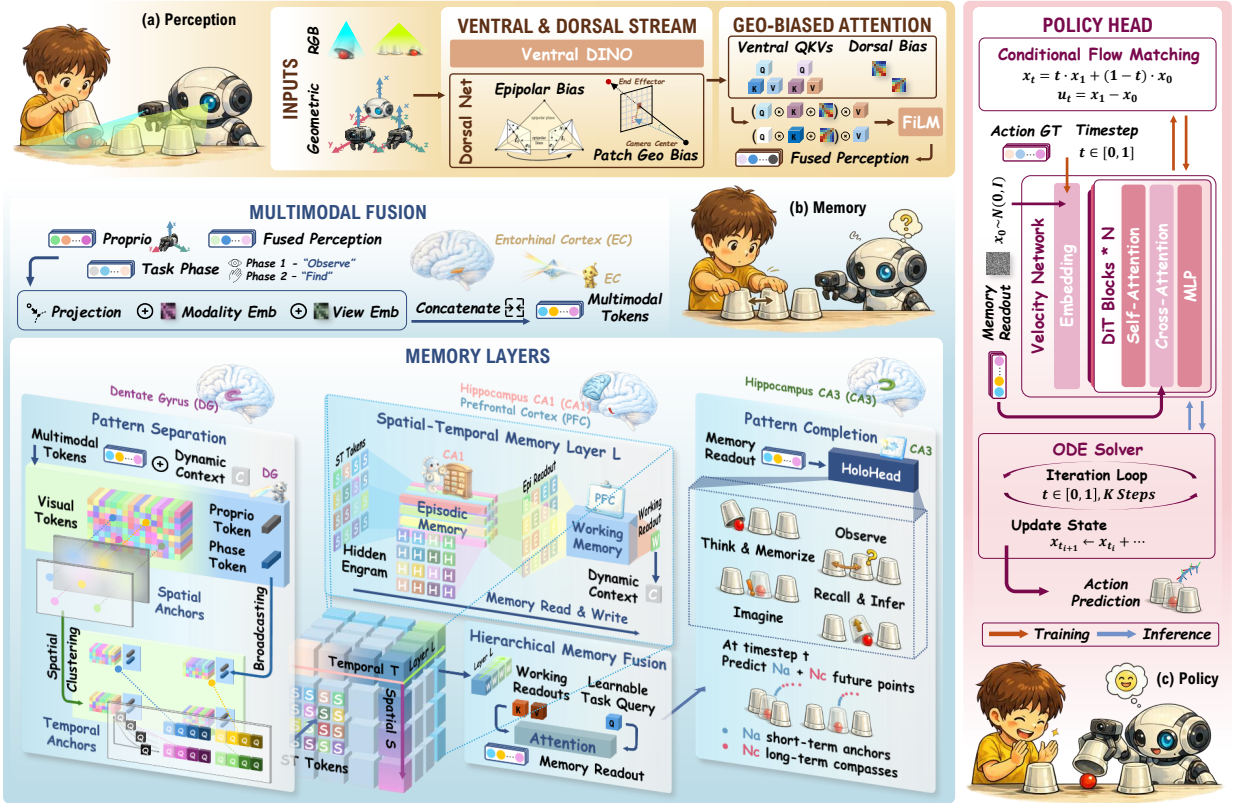


**Figure 2 Method overview.** Chameleon follows a Perception  $\rightarrow$  Memory  $\rightarrow$  Policy pipeline for long-horizon manipulation under perceptual aliasing. Perception produces geometry-grounded, view-consistent tokens that disambiguate observations before memory formation. Memory couples an episodic state with a working state and learns relevance-based recall through HoloHead rollout training. Conditioned on the memory readout, Policy samples a future end-effector pose trajectory via conditional flow matching for execution.

Policy samples  $\hat{x}_{t:t+H}$  and executes it using standard low-level inverse kinematics (IK) controllers.

*Perception  $\rightarrow$  Memory  $\rightarrow$  Policy.* As illustrated in Figure 2, our method follows a closed-loop pipeline:

$$\begin{aligned}
 x_t &= \Phi_{\text{perc}}(I_t^f, I_t^h, s_t, \psi_t), \\
 h_t &= \Phi_{\text{mem}}(x_t, h_{t-1}), \\
 \hat{x}_{t:t+H} &= \Phi_{\text{pol}}(h_t).
 \end{aligned} \tag{1}$$

Perception  $\Phi_{\text{perc}}$  converts the two camera views and proprioception into geometry-grounded, view-consistent patch tokens  $x_t$ , reducing ambiguity before memory formation (Section 3.2). Memory  $\Phi_{\text{mem}}$  couples an episodic state with a working state through fully differentiable dynamics and outputs a single decision state  $h_t$  that is the only interface to Policy (Section 3.3). This design directly targets the two challenges in Section 1. First, Memory supports disambiguated encoding so that perceptually similar situations can be written into distinct, in-

dexable traces, reducing interference. Second, Memory supports relevance-based recall so that retrieved content is selected for decision utility rather than perceptual similarity. We enforce goal-directed recall with HoloHead, an internal head trained with a latent imagination objective that compels the decision state to maintain and recall task-relevant memories. Conditioned only on  $h_t$ , Policy  $\Phi_{\text{pol}}$  generates the future end-effector pose trajectory via conditional flow matching (Section 3.4). The single-interface constraint makes the role of memory explicit: if the agent succeeds at long-horizon control, the information required for correct action selection must be represented in  $h_t$  and reliably propagated over time.

## 3.2 Perception

Perception implements the disambiguation requirement during memory formation: Decision states can be separated only if the sensory inputs (both visual and geometric) are encoded into sufficiently discriminative features. We write patch-level evidence from

two complementary views. The fixed front camera provides a stable global context, while the hand-mounted camera captures contact-scale details under occlusion. To prevent cross-view aggregation from mixing incompatible evidence, we use the EE pose as an action-centric geometric anchor that can be projected into both views to guide geometry-grounded cross-view communication (Figure 2 (a)).

*Inputs and output.* Given  $(I_t^f, I_t^h, s_t, \psi_t)$ , Perception outputs fused visual tokens  $x_t \in \mathbb{R}^{N \times d}$  for Memory.

*Ventral stream: patch appearance tokens.* For each view  $v \in \{f, h\}$ , a frozen DINO encoder produces patch tokens  $V_t^v = \text{DINO}(I_t^v) \in \mathbb{R}^{N_v \times d}$ .

*Dorsal stream: EE-anchored geometry codes.* From  $s_t$  we obtain the EE pose  $p_t \in \mathbb{R}^3$  and project it to each view as  $u_t^{\text{EE},v} = \Pi(K^v, T_t^v, p_t) \in \mathbb{R}^2$ . For patch  $i$  in view  $v$ , let  $u_{t,i}^v \in \mathbb{R}^2$  be the patch-center image coordinate and  $\tilde{u}_{t,i}^v \in \mathbb{P}^2$  its homogeneous form. We define the unit ray and the action-centric descriptor in one line:

$$\begin{aligned} r_{t,i}^v &= \frac{(K^v)^{-1} \tilde{u}_{t,i}^v}{\|(K^v)^{-1} \tilde{u}_{t,i}^v\|_2} \in \mathbb{R}^3, \\ g_{t,i}^v &= [u_{t,i}^v, r_{t,i}^v, \rho_{t,i}^v, \cos \theta_{t,i}^v] \in \mathbb{R}^7. \end{aligned} \quad (2)$$

Here  $\rho_{t,i}^v = \|u_{t,i}^v - u_t^{\text{EE},v}\|_2$  measures proximity to the EE projection. We define  $\cos \theta_{t,i}^v = r_{t,i}^{v\top} d_t^v$ , where  $d_t^v \in \mathbb{R}^3$  is the unit direction from the camera center to the EE pose in the camera frame, computed from  $(T_t^v, p_t)$  (details in Appendix). A geometric encoder outputs conditioning codes  $C_t^v \in \mathbb{R}^{N_v \times d_c}$  for feature modulation and unary patch biases  $b_t^v \in \mathbb{R}^{N_v}$  for attention gating, with  $b_{t,i}^v = \text{MLP}(g_{t,i}^v)$ .

*Geometry-biased bidirectional cross-view enhancement.* The front and hand views enhance each other through residual cross-attention. For attention from view  $a$  to view  $b$  with  $a \neq b$ , define  $Q = V_t^a W_Q$ ,  $K = V_t^b W_K$ , and  $U = V_t^b W_U$ , and update  $\bar{V}_t^a = V_t^a + \text{Attn}_{a \rightarrow b}(Q, K, U)$ . The attention logits combine an analytic epipolar feasibility bias and learned unary patch biases:

$$\begin{aligned} \text{Attn}_{a \rightarrow b}(Q, K, U) &= \text{softmax} \left( \frac{QK^\top}{\sqrt{d}} + B_{a \rightarrow b}^{\text{epi}} \right) \\ &\quad + b_t^a \mathbf{1}^\top + \mathbf{1}(b_t^b)^\top U. \end{aligned} \quad (3)$$

$B_{a \rightarrow b}^{\text{epi}} \in \mathbb{R}^{N_a \times N_b}$  is computed from the calibrated relative geometry using the fundamental matrix  $F_{a \rightarrow b}$  as

a negative point-to-epipolar-line distance (full form in Appendix). The unary term from  $b_t^v$  biases communication toward reliable, action-relevant patches derived from the EE anchor, without introducing an explicit pairwise matcher.

*Geometry-conditioned modulation and output.* We apply FiLM-style modulation and output fused evidence tokens:

$$\begin{aligned} \tilde{V}_t^v(i) &= \gamma(C_{t,i}^v) \odot \bar{V}_t^v(i) + \beta(C_{t,i}^v), \\ x_t &= \text{Concat}(\tilde{V}_t^f, \tilde{V}_t^h) \in \mathbb{R}^{N \times d}. \end{aligned} \quad (4)$$

This  $x_t$  preserves localized appearance evidence while restricting cross-view exchange to geometry-consistent correspondences, yielding a stable write-time evidence stream for Memory (Section 3.3).

### 3.3 Memory

Memory maps fused perception to a single readout decision state  $h_t$ . To reduce interference under perceptual aliasing, it encodes multimodal inputs with Spatial Anchors and Temporal Anchors, so evidence is written into a spatiotemporal state at multiple effective half-lives (i.e., encoded and stored across different time scales). Episodic Memory retains long-range traces, Working Memory integrates recalled context for immediate control, and HoloHead trains  $h_t$  to complete and maintain task-relevant information through imagination. This design follows the functional roles described in Section 1, from EC-style integration to DG-style separation, CA1 and PFC context maintenance, and CA3-style completion.

*Multimodal Fusion.* Memory consumes  $x_t \in \mathbb{R}^{N \times d}$  from Perception (Section 3.2), where  $x_t = \text{Concat}(\tilde{V}_t^f, \tilde{V}_t^h)$  and  $N = N_f + N_h$ . We form a proprioception token and, when available, a phase token as  $p_t = \text{Proj}_{\text{prop}}(s_t) \in \mathbb{R}^d$  and  $\varphi_t = E_{\text{phase}}[\psi_t] \in \mathbb{R}^d$ . We then add learned additive tags to preserve token identity across modalities and views:

$$\begin{aligned} \bar{x}_t^v &= \tilde{V}_t^v + A_{\text{vis}}^{\text{mod}} + A_v^{\text{view}}, \quad v \in \{f, h\}, \\ \bar{p}_t &= p_t + A_{\text{prop}}^{\text{mod}}, \\ \bar{\varphi}_t &= \varphi_t + A_{\text{phase}}^{\text{mod}}. \end{aligned} \quad (5)$$

Finally, we concatenate and normalize,

$$z_t = \text{LN}(\text{Concat}[\bar{x}_t^f, \bar{x}_t^h, \bar{p}_t, \bar{\varphi}_t]) \in \mathbb{R}^{M \times d}, \quad (6)$$

yielding fused tokens  $z_t$  for all layers. If  $\psi_t$  is unavailable, we omit  $\bar{\varphi}_t$  and set  $M = N + 1$ .

*Dynamic context modulation.* Each layer interprets the same fused evidence using the working context propagated from the previous layer. Let  $h_t^{(\ell-1)} \in \mathbb{R}^{d_w}$  be the working state output by layer  $\ell-1$  at time  $t$ , and let  $W_c^{(\ell)} \in \mathbb{R}^{d \times d_w}$  be a learned linear projection to token space. We broadcast-add the projected context to all tokens, where  $\mathbf{1} \in \mathbb{R}^M$  is an all-ones vector:

$$\tilde{z}_t^{(\ell)} = z_t + \mathbf{1} (W_c^{(\ell)} h_t^{(\ell-1)})^\top \in \mathbb{R}^{M \times d}. \quad (7)$$

*Spatial and Temporal Anchors.* Pattern separation begins by decomposing visual evidence into  $A$  spatial components. Let  $\bar{x}_t = \text{Concat}[\bar{x}_t^f, \bar{x}_t^h] \in \mathbb{R}^{N \times d}$  with  $N = N_f + N_h$ . Routing weights  $\pi_{t,a,i}^{(\ell)} \geq 0$  satisfy  $\sum_{a=1}^A \pi_{t,a,i}^{(\ell)} = 1$  and are produced by  $\pi_{t,\cdot,i}^{(\ell)} = \text{softmax}(\text{Router}^{(\ell)}(\bar{x}_{t,i}))$ . Each spatial anchor forms a visual summary and an anchor-specific token set by attaching shared global context:

$$u_{t,a}^{(\ell)} = \sum_{i=1}^N \pi_{t,a,i}^{(\ell)} \bar{x}_{t,i} \in \mathbb{R}^d, \quad (8)$$

$$\tilde{z}_t^{(\ell,a)} = \text{Concat}[u_{t,a}^{(\ell)}, \bar{p}_t, \bar{\varphi}_t] \in \mathbb{R}^{3 \times d}.$$

We then expand each spatial anchor output  $\tilde{z}_t^{(\ell,a)}$  into  $B$  temporal slots indexed by  $b$ , representing distinct characteristic half-lives in the subsequent state-space dynamics. With learned temporal queries  $\{q_{a,b}^{(\ell)}\}_{b=1}^B$ , the slot feature is

$$f_{t,a,b}^{(\ell)} = \text{Attn}(q_{a,b}^{(\ell)}, \tilde{z}_t^{(\ell,a)}) \in \mathbb{R}^d, \quad (9)$$

$$a = 1, \dots, A, \quad b = 1, \dots, B.$$

Collectively,  $\{f_{t,a,b}^{(\ell)}\}$  forms an  $A \times B$  spatiotemporal slot matrix, where  $a$  selects a spatial component and  $b$  selects a temporal resolution.

*Spatial-Temporal Memory with Episodic and Working States.* In layer  $\ell$ , each slot  $(a, b)$  maintains an episodic state  $m_{t,a,b}^{(\ell)}$ . The collection  $\{m_{t,a,b}^{(\ell)}\}$  forms the hidden engram, expressed only through readout. Given  $f_{t,a,b}^{(\ell)}$ , we compute

$$\theta_{t,a,b}^{(\ell)} = \text{Proj}_{a,b}^{(\ell)}(f_{t,a,b}^{(\ell)}), \quad (10)$$

where  $\theta_{t,a,b}^{(\ell)}$  follows a Mamba-style Gu and Dao (2024) selective state space model (SSM) parameterization with content-dependent input/readout factors and a step-size term. We assign each temporal index  $b \in \{1, \dots, B\}$  a distinct base step size  $\Delta t_b^{(0)}$  to implement an explicit half-life schedule, and further

modulate the effective step size by slot content via  $\text{Proj}_{a,b}^{(\ell)}$ . This yields a structured, content-adaptive multi-timescale memory, rather than a naive stack of  $A \times B$  identical SSMs. For efficiency, we implement a fused slot-wise scan that updates all  $A \times B$  states in a single pass. Episodic Memory updates the slot states by

$$m_{t,a,b}^{(\ell)} = \text{SSM}_{\text{epi}}^{(\ell)}(m_{t-1,a,b}^{(\ell)}; \theta_{t,a,b}^{(\ell)}), \quad (11)$$

and produces slot readouts  $r_{t,a,b}^{(\ell)} = \text{Read}_{\text{epi}}^{(\ell)}(m_{t,a,b}^{(\ell)}) \in \mathbb{R}^d$ . We aggregate these readouts into an episodic recall vector

$$r_t^{(\ell)} = \frac{1}{AB} \sum_{a=1}^A \sum_{b=1}^B W_{a,b}^{(\ell)} r_{t,a,b}^{(\ell)} \in \mathbb{R}^{d_w}, \quad (12)$$

and integrate it into Working Memory, which is the only output state of layer  $\ell$ :

$$h_t^{(\ell)} = \text{SSM}_{\text{work}}^{(\ell)}(h_{t-1}^{(\ell)}; \text{LN}(h_{t-1}^{(\ell)} + \text{Proj}_r^{(\ell)}(r_t^{(\ell)}))), \quad (13)$$

where  $h_t^{(\ell)} \in \mathbb{R}^{d_w}$ .

Input and readout is realized implicitly by state-space recursion: engram enters through working-state inputs, persists in episodic states, and is expressed through readouts, with no explicit retrieval gate required.

*Working Readout and Hierarchical Memory Fusion.* Layer  $\ell$  emits a Working Readout  $y_t^{(\ell)} = \text{LN}(W_o^{(\ell)} h_t^{(\ell)}) \in \mathbb{R}^{d_w}$ , where  $W_o^{(\ell)}$  is a learned linear projection. We fuse readouts from  $L$  layers with a task query  $q_{\text{task}} \in \mathbb{R}^{d_w}$ . We define the layer key  $k_{t,\ell} = U_\ell y_t^{(\ell)}$  and value  $v_{t,\ell} = \text{Enc}_\ell(y_t^{(\ell)})$ :

$$\alpha_{t,\ell} = \text{softmax}_\ell(\langle q_{\text{task}}, k_{t,\ell} \rangle), \quad (14)$$

$$h_t = \sum_{\ell=1}^L \alpha_{t,\ell} v_{t,\ell}.$$

The resulting  $h_t$  is the final Memory Readout consumed by Policy.

*HoloHead.* HoloHead enforces pattern completion via a latent imagination objective: conditioned on  $h_t$ , it predicts  $N_a + N_c$  waypoints in 2D (front-camera image-plane EE projection) and 3D (normalized world-frame EE pose).

$$\begin{bmatrix} \hat{w}_{t:t+N_a}^{2D} \\ \hat{w}_{t:t+N_c}^{2D} \\ \hat{w}_{t:t+N_a}^{3D} \\ \hat{w}_{t:t+N_c}^{3D} \end{bmatrix} = \text{HoloHead}(h_t). \quad (15)$$

and we supervise with

$$\mathcal{L}_{\text{holo}} = \sum_{\xi \in \{2D, 3D\}} \left( \|\hat{w}_{t:t+N_a}^{\xi} - w_{t:t+N_a}^{\xi}\|_1 + \|\hat{w}_{t:t+N_c}^{\xi} - w_{t:t+N_c}^{\xi}\|_1 \right). \quad (16)$$

This pressures the memory dynamics to reconstruct coherent futures from partial cues, leading to task-relevant retrieval. Details are provided in the Appendix.

### 3.4 Policy

Policy generates EE pose trajectory  $\hat{x}_{t:t+H} \in \mathbb{R}^{H \times d_{\text{raw}}}$  from the Memory Readout  $h_t$  (Section 3.3) for execution by low-level IK controllers.

*Single-state conditioning.* We condition the trajectory generator only on a projected token  $c_t = W_{\text{ctx}} h_t$ , where  $W_{\text{ctx}}$  is a learned linear projection.

*Conditional rectified flow matching.* Let  $x_1 \in \mathbb{R}^{H \times d_{\text{raw}}}$  be the ground-truth future trajectory and sample  $x_0 \sim \mathcal{N}(0, I)$  and  $\tau \sim \mathcal{U}(0, 1)$ . We define the interpolant  $x_{\tau} = (1 - \tau)x_0 + \tau x_1$  and target velocity  $u_{\tau} = x_1 - x_0$ , and train a velocity network  $v_{\theta}$  to predict  $u_{\tau}$  from  $(x_{\tau}, \tau, c_t)$ :

$$\hat{u}_{\tau} = v_{\theta}(x_{\tau}, \tau, c_t), \quad \mathcal{L}_{\text{flow}} = \mathbb{E}[\|\hat{u}_{\tau} - u_{\tau}\|^2], \quad (17)$$

where the loss is masked to ignore padded steps when trajectories have variable effective length. At inference, we sample  $\hat{x}_{t:t+H}$  by solving the ODE  $\dot{x} = v_{\theta}(x, \tau, c_t)$  from  $x(0) = x_0$  with a fixed-step solver.

## 4 Dataset

### 4.1 Memory-intensive Tasks Formulation

Intelligent agent decision-making arises from the interaction of goals, perception, memory, and prior knowledge, making fully memory-isolated tasks inherently unattainable. However, this interdependence opens a loophole that allows agents to exploit perceptual variations and bypass explicit memory retrieval. To assess whether agents truly possess long-term memory reasoning abilities, we construct a set of memory-intensive tasks that enforce a perceptually non-Markovian decision phase, where agents are required to make distinct decisions under identical visual observation (as shown in Figure 3) Chung et al. (2025); Cherepanov et al. (2025).

Building upon the biologically-inspired architecture formalized in Section 3, we develop **Camo-Dataset**, a comprehensive dataset designed to assess various dimensions of memory in robotic tasks. As shown in Table 1, we define three categories of memory tasks grounded in neuroscientific principles and aligned with prior robotics benchmarks Cherepanov et al. (2025).

### 4.2 Camo-Dataset

We design three robotic manipulation tasks to comprehensively evaluate three distinct memory abilities.

1. **Clean a specified plate.** This task simulates a kitchen scenario where a user puts a contaminated plate (e.g., used for raw meat but visually clean) for the robot to clean. This task exemplifies an event-object binding problem, requiring the agent to associate a specific event with an identical object.
2. **Play shell game.** This task simulates a shell game in which the user hides a cube under one cup and randomly swaps the cups. The robot must track the hidden cube through memory. This task represents spatial tracking problems, such as organizing containers or retrieving items from drawers.
3. **Add various seasonings.** This task simulates sequentially adding three seasonings during cooking. After each addition, the robot must return the seasoning to its original position and move back to a preparation pose, making it impossible to infer whether a seasoning has already been added without recalling prior actions. This task represents counting or sequential execution problems, such as making coffee or baking a cake.

## 5 Experiment Result

### 5.1 Experiment Setup

*Dataset.* We evaluate Chameleon on Camo-Dataset under a consistent training and deployment pipeline with real-world robotic execution. For each task, we collect 120 teleoperated demonstrations using a UR5e robotic arm under human-in-the-loop control to ensure task execution quality. During the test phase, the trained model is deployed on the same physical UR5e robot, where it performs 36 independent real-world trials for each task category. We use the same decision setup and candidate sampling in the dataset and in real-robot evaluation, so the

**Table 1** Three memory categories derived based on cognitive science, along with corresponding biological substrates and tasks in Camo-Dataset.

| Category          | Characteristics   | Biological Correspondence    | Task                     |
|-------------------|---|------------------------------|--------------------------|
| <b>Episodic</b>   | Introduces transient variables that disrupt habitual patterns.                | HC-centered episodic memory. | Clean a specified plate. |
| <b>Spatial</b>    | Maintains and updates occluded object locations using environmental geometry. | EC-HC cognitive map.         | Play shell game.         |
| <b>Sequential</b> | Tracks temporally ordered sub-goals to prevent repetition or omission.        | PFC-centered working memory. | Add various seasonings.  |

**Table 2** Performance (DSR ( $\kappa$ ), MSR, SR, and CSR in %) across three task categories for two baselines, Chameleon, and its ablated models (36 tasks for each category). Best results are highlighted in blue, and second-best results are highlighted in pink. Module\* denotes the variant in which we replace our Memory module with Module.

| Method  | Episodic ( $p_e = 1/3$ ) |      |      |       | Spatial ( $p_e = 1/3$ ) |      |      |      | Sequential ( $p_e = 1/27$ ) |      |      |      |
|---|--------------------------|------|------|-------|-------------------------|------|------|------|-----------------------------|------|------|------|
|   | DSR ( $\kappa$ )         | MSR  | SR   | CSR   | DSR ( $\kappa$ )        | MSR  | SR   | CSR  | DSR ( $\kappa$ )            | MSR  | SR   | CSR  |
| <b>Diffusion Policy</b> Chi et al. (2023)     | 33.3 (0.0)               | 91.7 | 30.6 | 30.0  | 34.3 (1.4)              | 97.2 | 33.3 | 31.7 | 0.0 (-3.8)                  | 13.9 | 0.0  | 6.7  |
| <b>Flow Matching</b> Zhang and Gienger (2024) | 30.0 (-5.0)              | 83.3 | 25.0 | 35.0  | 25.7 (-11.4)            | 97.2 | 25.0 | 35.0 | 0.0 (-3.8)                  | 5.6  | 0.0  | 8.3  |
| <b>ACT</b> Zhao et al. (2023)                 | 28.0 (-8.0)              | 83.3 | 19.4 | 28.3  | 35.5 (3.2)              | 86.1 | 30.6 | 36.7 | NA (NA)                     | 0.0  | 0.0  | 10.0 |
| <b>Chameleon</b>                              | 100.0 (100.0)            | 86.1 | 86.1 | 100.0 | 73.5 (60.3)             | 94.4 | 69.4 | 91.7 | 72.2 (71.2)                 | 50.0 | 36.1 | 85.0 |
| <b>w/o Memory</b>                             | 37.0 (5.6)               | 75.0 | 27.8 | 36.7  | 34.5 (1.7)              | 80.6 | 27.8 | 35.0 | 0.0 (-3.8)                  | 8.3  | 0.0  | 6.7  |
| <b>Memory Bank*</b>                           | NA (NA)                  | 0.0  | 0.0  | 33.3  | NA (NA)                 | 0.0  | 0.0  | 31.7 | NA (NA)                     | 0.0  | 0.0  | 11.7 |
| <b>Vanilla Mamba*</b>                         | 28.0 (-8.0)              | 69.4 | 19.4 | 31.7  | 30.3 (-4.5)             | 91.7 | 27.8 | 28.3 | 0.0 (-3.8)                  | 44.4 | 0.0  | 8.3  |
| <b>w/o Dorsal Stream</b>                      | 96.8 (95.2)              | 86.1 | 83.3 | 100.0 | 51.5 (27.3)             | 91.7 | 47.2 | 65.0 | 66.7 (65.4)                 | 41.7 | 27.8 | 71.7 |
| <b>w/o HoloHead</b>                           | 60.7 (41.1)              | 77.8 | 47.2 | 61.7  | 46.7 (20.0)             | 83.3 | 38.9 | 53.3 | 0.0 (-3.8)                  | 33.3 | 0.0  | 13.3 |

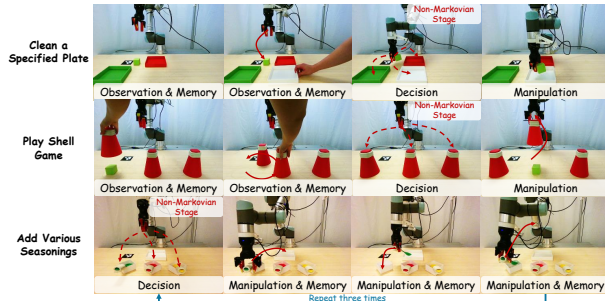


**Figure 3** Illustration of task execution in Camo-Dataset. **Clean a specified plate:** the agent remembers the user’s newly placed plate. At the decision stage, three plates are similar. **Play shell game:** the agent tracks the cup covering the cube. At the decision stage, the three cups appear identical. **Add various seasonings:** the agent recalls which spoon was picked up. At the decision stage, the three spoons are similar.

chance-level success probability is the same in both settings.

*Baseline.* We compare Chameleon against three state-of-the-art embodied agent models, Diffusion Policy Chi et al. (2023), Flow Matching Zhang and Gienger (2024), and ACT Zhao et al. (2023). We conduct ablation studies to analyze the contribution of key components by evaluating five variants. The parameter counts of all models are reported in the

Appendix.

*Metrics.* Beyond the standard *Success Rate (SR)*, we introduce *Decision Success Rate (DSR)* and *Manipulation Success Rate (MSR)* to provide finer-grained evaluation of memory-intensive tasks, measuring retrieval accuracy and execution success, respectively. These metrics satisfy  $SR = DSR \times MSR$ . Since DSR is subject to chance-level performance, we adopt the chance-adjusted *Cohen’s kappa coefficient* Cohen (1960) to reflect memory-dependent decision success rate:

$$\kappa = \frac{p_o - p_e}{1 - p_e}, \quad (18)$$

where  $p_o$  is DSR and  $p_e$  is the chance-level DSR.

*Implementation Details.* For each task, we train using AdamW with learning rate  $1 \times 10^{-4}$ , batch size 4, cosine annealing, and bfloat16 mixed precision. Training runs for 20K steps on a single 4090 GPU. For inference, trajectories are generated using 50 rectified-flow ODE steps. The average end-to-end inference latency is 82 ms per control step, enabling real-time manipulation on the UR5e platform. All architectural hyperparameters, configurations, and training details are further provided in the Appendix.

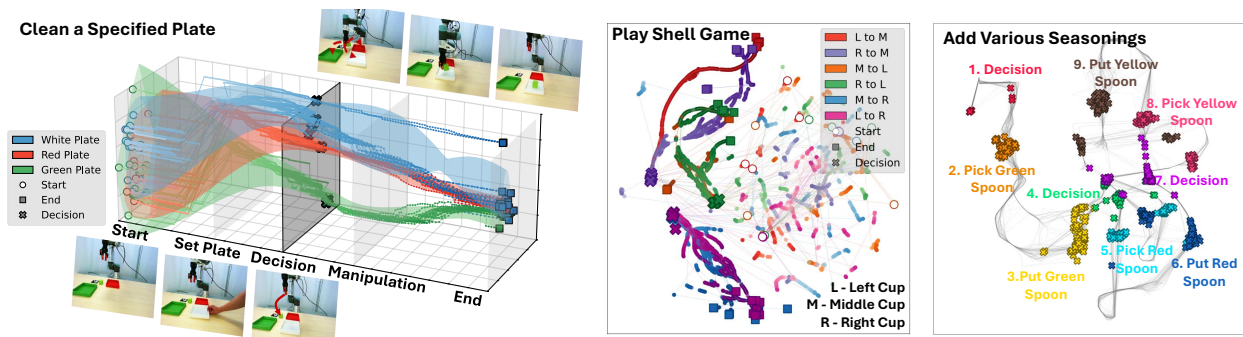


**Figure 4** Pattern separation in the decision state. UMAP projections of  $h_t$  for all three task categories, colored by the latent decision target. Clear clustering under visually aliasing indicates that  $h_t$  disambiguates the history-dependent state.

## 5.2 Comprehensive Systematic Study

**Chameleon achieves near-perfect decision success rate in episodic recall.** As shown in Table 2, Chameleon attains 100.0% (100.0%) in DSR ( $\kappa$ ), 86.1% in SR, and 86.1% in MSR, consistently outperforming baselines on memory-driven decision. Compared to Diffusion Policy, a representative baseline, it improves DSR ( $\kappa$ ) by 66.7% (100%) and SR by 55.5%, while exhibiting a marginal decrease of 5.6% in MSR. These results highlight Chameleon’s superior episodic representation and task-relevant retrieval capability.

**Chameleon maintains strong spatial tracking performance under memory constraints.** It achieves 73.5% (60.3%), 94.4%, and 69.4% in DSR ( $\kappa$ ), MSR, and SR, respectively, while Diffusion Policy underperforms by 39.2% (58.9%) and 36.1% in DSR ( $\kappa$ ) and SR, with a slight increase of 2.8% in MSR. These results indicate that Chameleon maintains stable spatial tracking across three object rearrangements by selectively recalling relevant past experiences.

**Chameleon further sustains an advantage in sequential tasks that require consistent decisions across multiple stages.** In this task, Chameleon achieves 72.2% (71.2%), 50.0%, and 36.1% in DSR ( $\kappa$ ), MSR, and SR, respectively, while Diffusion Policy degrades substantially across all three metrics by 72.2% (75%), 36.1%, and 36.1%, respectively. This suggests that structured memory helps maintain task progression over long sequences and can better preserve execution accuracy in multi-step and action-intensive tasks.

## 5.3 Ablation Study

We ablate core components of Chameleon under the same training and real-robot evaluation protocol as Table 2. Implementation details are provided in Appendix. In addition to the metrics above, we report the *classification success rate (CSR)*, the precision of

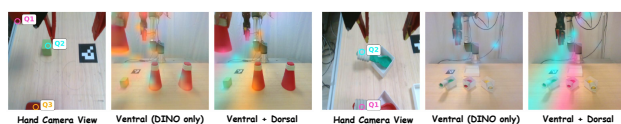


**Figure 5** Dorsal stream enables write-time disambiguation. Cross-view attention in the spatial task: with the dorsal stream, attention focuses on the correct target via end-effector geometry and epipolar feasibility; without it, attention diffuses across distractors, degrading downstream memory and execution.

a linear probe trained on the frozen decision-stage state  $h_t$  to predict the latent decision target under aliasing.

**Continuous and structured memory is necessary for non-Markovian decision-making.** The reactive variant **w/o Memory** collapses, confirming that the benchmark is non-Markovian at the observation level. A **Memory Bank** with similarity-based retrieval remains near chance-level on CSR, indicating that discrete retrieval is unreliable under aliasing because visually plausible recalls can be decision-irrelevant. In contrast, Chameleon integrates history through continuous state dynamics and consistently improves DSR and CSR across all task categories (Table 2). These gains are not attributable to recurrence alone. **Vanilla Mamba** degrades most on sequential tasks, suggesting long-horizon temporal interference without our anchor-structured, multi-timescale episodic state, which reduces interference and improves both decision reliability and end-to-end success.

**Write-time spatial disambiguation is necessary for robust tracking.** Ablating the dorsal geometry pathway (**w/o Dorsal Stream**) substantially reduces MSR and SR on the spatial category (Table 2). As visualized in Figure 5, the full model concentrates cross-view attention onto the physically correct target using end-

effector anchored geometry and epipolar feasibility, whereas removing the dorsal stream yields diffuse attention across distractors, weakening the evidence written into memory.

**HoloHead stabilizes the decision state representation.**

The **w/o HoloHead** variant reduces DSR and CSR despite comparable capacity (Table 2), indicating that the latent imagination objective is essential for keeping  $h_t$  from collapsing to instantaneous appearance and for preserving a predictive, decision-sufficient representation under aliasing.

**5.4 Qualitative Mechanistic Validation**

To verify whether the decision state  $h_t$  achieves the intended design of event-biased separation, and goal-directed recall (Section 3), we project high-dimensional states  $h_t$  into a low-dimensional manifold with UMAP, and probe its generative behavioral readout via HoloHead’s predictive rollouts.

**Pattern separation.** As shown in Figure 4, in episodic and spatial tasks, the introduction of memory information causes  $h_t$  to separate from overlapping clusters into distinct manifolds corresponding to different latent states. Importantly, these manifolds remain stable even after the disambiguating visual evidence disappears, indicating that the representation preserves event- and location-level distinctions. In sequential tasks,  $h_t$  instead evolves along different stages of a shared manifold as the task progresses, reflecting the maintenance of temporal process information.

**Pattern completion.** Pattern completion refers to recovering a task-relevant latent state in  $h_t$  from partial cues. Since the latent state is not directly observable, we assess it through predictive rollouts generated from  $h_t$ . If  $h_t$  captures the task-relevant latent state, the predicted trajectory should remain consistent with the intended target behavior. As shown in Figure 6, rollouts from randomly selected timesteps across three tasks remain goal-consistent,

supporting that  $h_t$  encodes task-relevant state for pattern completion.

**6 Conclusion**

We study memory-intensive robot manipulation under perceptual aliasing, where decision-time observations are insufficient and history is required, yielding non-Markovian decision points in observation level. Inspired by human episodic memory, we propose Chameleon, a differentiable memory architecture that couples disambiguating memory writing with goal-directed recall. On our proposed Camo-Dataset, real-robot experiments and representation analyses show improved robustness and long-horizon control.

*Limitations and Future Work.* Chameleon focuses on learnable episodic memory for perception-driven manipulation and does not incorporate the semantic abstractions used by many Vision–Language–Action (VLAs) for broad zero-shot generalization. Our experiments use a single robot platform, leaving cross-embodiment transfer and learning event segmentation as future work. An important direction is to integrate the episodic memory stack with foundation models to combine structural encoding with higher-level priors for open-world autonomy.

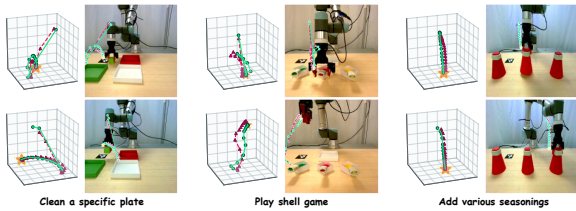


**Figure 6 Pattern completion via predictive rollouts.** HoloHead waypoint predictions at the decision stage remain consistent with the latent target under ambiguity, indicating that  $h_t$  supports completion from partial cues.

## References

- Timothy A Allen and Norbert J Fortin. The evolution of episodic memory. *Proceedings of the National Academy of Sciences*, 110(supplement\_2):10379–10386, 2013.
- Tarek Amer and Lila Davachi. Extra-hippocampal contributions to pattern separation. *elife*, 12:e82250, 2023.
- Abrar Anwar, John Welsh, Joydeep Biswas, Soha Pouya, and Yan Chang. Remembr: Building and reasoning over long-horizon spatio-temporal memory for robot navigation. In *2025 IEEE International Conference on Robotics and Automation (ICRA)*, pages 2838–2845. IEEE, 2025.
- Arnold Bakker, C Brock Kirwan, Michael Miller, and Craig EL Stark. Pattern separation in the human hippocampal ca3 and dentate gyrus. *science*, 319(5870):1640–1642, 2008.
- Sebastian Borgeaud, Arthur Mensch, Jordan Hoffmann, Trevor Cai, Eliza Rutherford, Katie Millican, George Bm Van Den Driessche, Jean-Baptiste Lespiau, Bogdan Damoc, Aidan Clark, et al. Improving language models by retrieving from trillions of tokens. In *International conference on machine learning*, pages 2206–2240. PMLR, 2022.
- Egor Cherepanov, Nikita Kachaev, Alexey K Kovalev, and Aleksandr I Panov. Memory, benchmark & robots: A benchmark for solving complex tasks with reinforcement learning. *arXiv preprint arXiv:2502.10550*, 2025.
- Cheng Chi, Siyuan Feng, Yilun Du, Zhenjia Xu, Eric Cousineau, Benjamin Burchfiel, and Shuran Song. Diffusion policy: Visuomotor policy learning via action diffusion. In *Proceedings of Robotics: Science and Systems (RSS)*, 2023.
- Nhat Chung, Taisei Hanyu, Toan Nguyen, Huy Le, Frederick Bumgarner, Duy Minh Ho Nguyen, Khoa Vo, Kashu Yamazaki, Chase Rainwater, Tung Kieu, et al. Rethinking progression of memory state in robotic manipulation: An object-centric perspective. *arXiv preprint arXiv:2511.11478*, 2025.
- Jacob Cohen. A coefficient of agreement for nominal scales. *Educational and psychological measurement*, 20(1):37–46, 1960.
- Bradford C Dickerson and Howard Eichenbaum. The episodic memory system: neurocircuitry and disorders. *Neuropsychopharmacology*, 35(1):86–104, 2010.
- Jinyuan Fang, Zaiqiao Meng, and Craig Macdonald. Trace the evidence: Constructing knowledge-grounded reasoning chains for retrieval-augmented generation. In *Findings of the Association for Computational Linguistics: EMNLP 2024*, pages 8472–8494, 2024.
- YukTungSamuel Fang, Zhikang Shi, Jiabin Qiu, Zixuan Chen, Jieqi Shi, Hao Xu, Jing Huo, and Yang Gao. Inherit-sg: Incremental hierarchical semantic scene graphs with rag-style retrieval. *arXiv preprint arXiv:2602.12971*, 2026.
- Pascale Fung, Yoram Bachrach, Asli Celikyilmaz, Kamalika Chaudhuri, Delong Chen, Willy Chung, Emmanuel Dupoux, Hongyu Gong, Hervé Jégou, Alessandro Lazaric, et al. Embodied ai agents: Modeling the world. *arXiv preprint arXiv:2506.22355*, 2025.
- Luyu Gao, Xueguang Ma, Jimmy Lin, and Jamie Callan. Precise zero-shot dense retrieval without relevance labels. In *Proceedings of the 61st Annual Meeting of the Association for Computational Linguistics (Volume 1: Long Papers)*, pages 1762–1777, 2023.
- Albert Gu and Tri Dao. Mamba: Linear-time sequence modeling with selective state spaces. In *First conference on language modeling*, 2024.
- Bernal Jimenez Gutierrez, Yiheng Shu, Yu Gu, Michihiro Yasunaga, and Yu Su. Hipporag: Neurobiologically inspired long-term memory for large language models. *Advances in Neural Information Processing Systems*, 37:59532–59569, 2024.
- Vladimir Karpukhin, Barlas Oguz, Sewon Min, Patrick Lewis, Ledell Wu, Sergey Edunov, Danqi Chen, and Wen-tau Yih. Dense passage retrieval for open-domain question answering. In *Proceedings of the 2020 conference on empirical methods in natural language processing (EMNLP)*, pages 6769–6781, 2020.
- Patrick Lewis, Ethan Perez, Aleksandra Piktus, Fabio Petroni, Vladimir Karpukhin, Naman Goyal, Heinrich Küttler, Mike Lewis, Wen-tau Yih, Tim Rocktäschel, et al. Retrieval-augmented generation for knowledge-intensive nlp tasks. *Advances in neural information processing systems*, 33:9459–9474, 2020.
- Min Lin, Xiwen Liang, Bingqian Lin, Liu Jingzhi, Zijian Jiao, Kehan Li, Yuhan Ma, Yuecheng Liu, Shen Zhao, Yuzheng Zhuang, et al. Echovla: Robotic vision-language-action model with synergistic declarative memory for mobile manipulation. *arXiv preprint arXiv:2511.18112*, 2025.
- Peiran Liu, Qiang Zhang, Daojie Peng, Lingfeng Zhang, Yihao Qin, Hang Zhou, Jun Ma, Renjing Xu, and Yiding Ji. Toponav: Topological graphs as a key enabler for advanced object navigation. *arXiv preprint arXiv:2509.01364*, 2025.
- Yang Liu, Xinchuai Song, Kaixuan Jiang, Weixing Chen, Jingzhou Luo, Guanbin Li, and Liang Lin. Meia: Multimodal embodied perception and interaction in unknown environments. *arXiv preprint arXiv:2402.00290*, 2024.
- Alex Mallen, Akari Asai, Victor Zhong, Rajarshi Das, Daniel Khashabi, and Hannaneh Hajishirzi. When not to trust language models: Investigating effectiveness of parametric and non-parametric memories. In *Proceedings of the 61st annual meeting of the association*

- for computational linguistics (volume 1: Long papers), pages 9802–9822, 2023.
- Ruaridh Mon-Williams, Gen Li, Ran Long, Wenqian Du, and Christopher G Lucas. Embodied large language models enable robots to complete complex tasks in unpredictable environments. *Nature Machine Intelligence*, 7(4):592–601, 2025.
- Chi T Ngo, Sebastian Michelmann, Ingrid R Olson, and Nora S Newcombe. Pattern separation and pattern completion: Behaviorally separable processes? *Memory & Cognition*, 49(1):193–205, 2021.
- Joon Sung Park, Joseph O’Brien, Carrie Jun Cai, Meredith Ringel Morris, Percy Liang, and Michael S Bernstein. Generative agents: Interactive simulacra of human behavior. In *Proceedings of the 36th annual acm symposium on user interface software and technology*, pages 1–22, 2023.
- Larry R Squire. Memory and the hippocampus: a synthesis from findings with rats, monkeys, and humans. *Psychological review*, 99(2):195, 1992.
- Weihang Su, Yichen Tang, Qingyao Ai, Junxi Yan, Changyue Wang, Hongning Wang, Ziyi Ye, Yujia Zhou, and Yiqun Liu. Parametric retrieval augmented generation. In *Proceedings of the 48th International ACM SIGIR Conference on Research and Development in Information Retrieval*, pages 1240–1250, 2025.
- Timothy J Teyler and Pascal DiScenna. The hippocampal memory indexing theory. *Behavioral neuroscience*, 100(2):147, 1986.
- Yuwei Wan, Zheyuan Chen, Ying Liu, Chong Chen, and Michael Packianather. Empowering llms by hybrid retrieval-augmented generation for domain-centric q&a in smart manufacturing. *Advanced Engineering Informatics*, 65:103212, 2025.
- Zixuan Wang, Bo Yu, Junzhe Zhao, Wenhao Sun, Sai Hou, Shuai Liang, Xing Hu, Yinhe Han, and Yiming Gan. Karma: Augmenting embodied ai agents with long-and-short term memory systems. In *2025 IEEE International Conference on Robotics and Automation (ICRA)*, pages 1–8. IEEE, 2025.
- Ella Worsfold, Nicola S Clayton, and Lucy G Cheke. Revisiting episodic-like memory in scrub jays: Is there more we can still learn from what–where–when caching behaviour? *Learning & Behavior*, 53(1):65–79, 2025.
- Quanting Xie, So Yeon Min, Pengliang Ji, Yue Yang, Tianyi Zhang, Kedi Xu, Aarav Bajaj, Ruslan Salakhutdinov, Matthew Johnson-Roberson, and Yonatan Bisk. Embodied-rag: General non-parametric embodied memory for retrieval and generation. *arXiv preprint arXiv:2409.18313*, 2024.
- Shunyu Yao, Jeffrey Zhao, Dian Yu, Nan Du, Izhak Shafran, Karthik R Narasimhan, and Yuan Cao. React: Synergizing reasoning and acting in language models. In *The eleventh international conference on learning representations*, 2022.
- Fan Zhang and Michael Gienger. Affordance-based robot manipulation with flow matching. *arXiv preprint arXiv:2409.01083*, 2024.
- Tony Z Zhao, Vikash Kumar, Sergey Levine, and Chelsea Finn. Learning fine-grained bimanual manipulation with low-cost hardware. In *ICML Workshop on New Frontiers in Learning, Control, and Dynamical Systems*, 2023.
- Yicong Zheng, Nora Wolf, Charan Ranganath, Randall C O’Reilly, and Kevin L McKee. Flexible prefrontal control over hippocampal episodic memory for goal-directed generalization. *arXiv preprint arXiv:2503.02303*, 2025.
- Yichen Zhu, Zhicai Ou, Xiaofeng Mou, and Jian Tang. Retrieval-augmented embodied agents. In *Proceedings of the IEEE/CVF Conference on Computer Vision and Pattern Recognition*, pages 17985–17995, 2024.

# Supplementary Material

## Chameleon: Episodic Memory for Long-Horizon Robotic Manipulation

### Table of Contents

Within this supplementary material, we elaborate on the following aspects:

- **Appendix A: Additional Method Details**
  - **A.1:** Overview and Problem Setup
  - **A.2:** Perception
  - **A.3:** Memory
  - **A.4:** Policy
- **Appendix B: Additional Experimental Details**
  - **B.1:** Camo-Dataset Statistics
  - **B.2:** Implementation Details
  - **B.3:** Model Size and Computational Cost of Experiment
  - **B.4:** Evaluation Metrics Definitions
  - **B.5:** Failure Case Analysis
- **Appendix C: Human Episodic Memory and Correspondence to Chameleon**
  - **C.1:** Overview of the EC–HC–PFC Episodic Memory Circuit
  - **C.2:** Perceptual Pathways: Ventral and Dorsal Streams
  - **C.3:** Entorhinal Cortex: Interface Between Perception and Memory
  - **C.4:** Hippocampus: Pattern Separation and Pattern Completion
  - **C.5:** Hippocampus–Prefrontal Cortex Interaction

## A Additional Method Details

### A.1 Overview and Problem Setup

*Problem setup.* We study long-horizon robotic manipulation under partial observability, where correct control depends on information that may be occluded, transient, or only established by earlier interactions. At each timestep  $t$ , the agent receives a multimodal observation  $o_t = \{I_t^f, I_t^h, s_t, \psi_t\}$ , where  $I_t^f$  and  $I_t^h$  are RGB images from a fixed front camera and a hand-mounted side camera,  $s_t$  denotes the robot proprioceptive state (including end-effector pose and gripper state), and  $\psi_t$  is an optional task-stage signal (e.g., a phase ID). Instead of predicting a single-step command, we parameterize decision making by generating a *future end-effector pose trajectory* over a horizon  $H$  (Section 3.4). During training, we supervise the model with ground-truth future pose states  $x_{t:t+H} \in \mathbb{R}^{H \times d_{\text{raw}}}$ ; during inference, the policy samples  $\hat{x}_{t:t+H}$  from a conditional generative model and executes it with standard low-level controllers. This trajectory-level target makes long-horizon structure explicit and mitigates compounding errors typical of step-wise prediction.

*Core challenge.* Long-horizon manipulation contains decision points where instantaneous perception is insufficient: the agent must act differently under nearly identical sensory inputs because the disambiguating variables are historical, occluded, or fleeting. Equivalently, there exist timesteps where optimal control cannot be expressed as a function of  $o_t$  alone, making the problem non-Markovian in observation space and requiring an internal state that carries missing context forward. We therefore center our design on a *decision-sufficient* memory state  $h_t$  that serves as the sole interface between perception and control. Importantly,  $h_t$  is not a passive summary; it is a recurrent control state that fuses (i) *past* traces needed to resolve hidden causes, (ii) *present* evidence needed to ground the current situation, and (iii) *future* constraints that keep the state predictively coherent for near-term evolution. In our framework, retention and selection are realized implicitly through continuous state dynamics and a single task-adaptive readout, avoiding discrete database-style retrieval. To ensure that  $h_t$  remains actionable rather than merely compressive, we further regularize it with imagination-style rollout supervision, which pressures the memory state to support internal rollouts consistent with the agent’s subsequent behavior.

*Overview.* As illustrated in Figure 7, our method instantiates a closed-loop pipeline with clean interfaces,

*Perception*  $\rightarrow$  *Memory*  $\rightarrow$  *Policy*:

$$x_t = \Phi_{\text{perc}}(I_t^f, I_t^h, s_t, \psi_t), \quad (19)$$

$$h_t = \Phi_{\text{mem}}(x_t, h_{t-1}), \quad (20)$$

$$\hat{x}_{t:t+H} = \Phi_{\text{pol}}(h_t), \quad (21)$$

where perception constructs geometry-grounded, view-consistent patch tokens  $x_t$  to reduce ambiguity before memory formation (Section 3.2), memory transforms multimodal evidence into a compact recurrent state and outputs a single readout  $h_t$  shaped by rollout supervision (Section 3.3), and policy generates the future pose trajectory via conditional flow matching conditioned only on  $h_t$  (Section 3.4). This single-readout interface turns sufficiency into an architectural constraint: if the agent succeeds in long-horizon control, it must be mediated through the informativeness and stability of the learned memory state. At a high level, the resulting organization is bio-inspired in its division of labor across perception, memory, and control, while remaining fully differentiable and end-to-end trainable.

### A.2 Perception

Long-horizon manipulation requires memory to disambiguate situations that can look similar at a glance. This is only possible if perception exposes localized evidence, because a single global summary tends to discard fine-grained cues (object parts, boundaries, contact regions) that later resolve ambiguity. We therefore provide memory with a patch-level evidence set from two complementary viewpoints: a fixed front camera captures stable global context, while a hand-mounted camera reveals close-range details during contact-rich interactions. The central difficulty is correspondence: the same physical region can shift substantially in the image plane and undergo view-dependent occlusion. If the two streams are written into memory without alignment, temporal aggregation can mix incompatible evidence. Our key idea is to use the end-effector (EE) as an action-centric geometric anchor. The EE pose is directly known in 3D from proprioception and can be projected into each view, providing a reliable 2D–3D bridge to ground cross-view correspondence and to emphasize control-relevant regions. This design follows a bio-inspired dorsal–ventral division of labor: a ventral pathway provides rich appearance evidence (what), while a dorsal pathway injects action-centric spatial structure (where/how) before memory integration.

*Inputs and output.* At timestep  $t$ , perception receives two RGB images  $I_t^f$  (front) and  $I_t^h$  (hand), robot state  $s_t$  (including EE pose and gripper state),

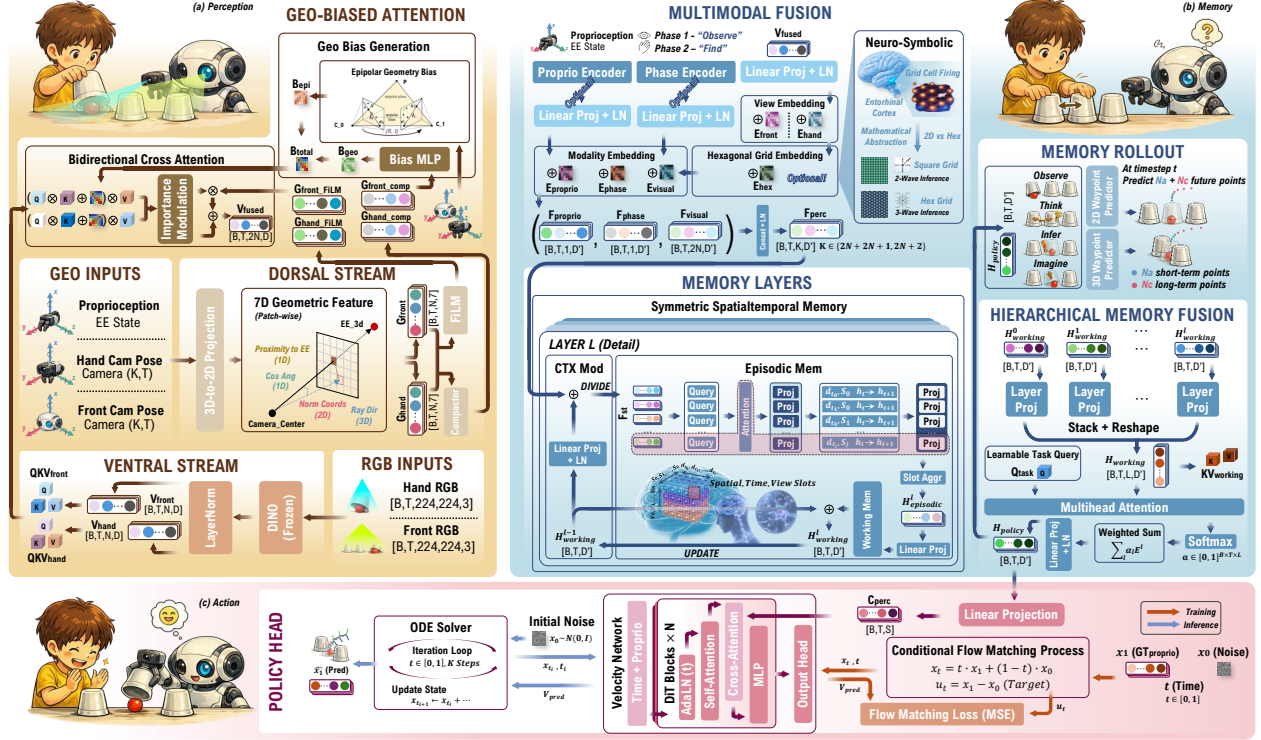


**Figure 7 Method overview.** Our system follows a closed-loop *perception–memory–policy* pipeline for long-horizon manipulation. **(a) Perception:** from front/hand RGB, we construct geometry-grounded, view-consistent patch tokens that reduce ambiguity *before* memory formation. **(b) Memory:** multimodal evidence is transformed into a compact recurrent decision state via iterative updates and a *single* learned readout, further shaped by imagination-style rollout supervision. **(c) Policy:** conditioned *only* on this memory readout, a conditional flow-matching generator produces the future end-effector pose trajectory for execution.

and an optional stage signal  $\psi_t$ . It outputs a token set

$$x_t \in \mathbb{R}^{N \times d}, \quad (22)$$

which serves as the visual evidence stream for the memory module.

*Ventral stream:* appearance evidence from a frozen DINO encoder. For each view  $v \in \{f, h\}$ , we extract patch-level appearance tokens using a frozen DINO backbone:

$$V_t^v = \text{DINO}(I_t^v) \in \mathbb{R}^{N_v \times d}, \quad (23)$$

where  $N_v$  is the number of patch tokens for view  $v$ . This preserves detailed local evidence while leveraging strong pretrained visual priors.

*Dorsal stream:* EE-anchored geometric features. Let  $K^v$  and  $T_t^v \in SE(3)$  denote the camera intrinsics and world-to-camera extrinsics for view  $v$  (with  $T_t^h$  varying with the EE for the hand-mounted camera). From  $s_t$  we obtain the EE position  $p_t \in \mathbb{R}^3$  in the

world frame and compute its projection in each view:

$$u_t^{\text{EE},v} = \Pi(K^v, T_t^v, p_t) \in \mathbb{R}^2. \quad (24)$$

For each patch  $i$  in view  $v$ , let  $u_{t,i}^v \in \mathbb{R}^2$  be the normalized image coordinate of the patch center and  $\tilde{u}_{t,i}^v \in \mathbb{P}^2$  its homogeneous coordinate. We define the corresponding unit ray direction in the camera frame by

$$r_{t,i}^v = \frac{(K^v)^{-1} \tilde{u}_{t,i}^v}{\|(K^v)^{-1} \tilde{u}_{t,i}^v\|_2} \in \mathbb{R}^3, \quad (25)$$

Following Figure 7, we form a raw action-centric descriptor

$$g_{t,i}^v = [u_{t,i}^v, r_{t,i}^v, \rho_{t,i}^v, \cos \theta_{t,i}^v] \in \mathbb{R}^7, \quad (26)$$

where  $\rho_{t,i}^v = \|u_{t,i}^v - u_t^{\text{EE},v}\|_2$  measures proximity to the EE projection (action relevance in the image), and  $\cos \theta_{t,i}^v$  captures viewing geometry between the patch ray and the EE direction induced by  $(p_t, T_t^v)$ . A geometric encoder produces compact conditioning features  $C_t^v \in \mathbb{R}^{N_v \times d_c}$  for modulation and patch-wise raw descriptors  $G_t^v \in \mathbb{R}^{N_v \times 7}$  for bias prediction.

*Geometry-biased bi-directional cross-view enhancement.* We do not collapse the two views into a single representation. Instead, we enhance each view with geometrically compatible evidence from the other view through residual, bi-directional cross-attention. For attention from view  $a$  to view  $b$  (with  $a \neq b$ ), define projected queries/keys/values

$$Q_t^a = V_t^a W_Q, \quad K_t^b = V_t^b W_K, \quad U_t^b = V_t^b W_V, \quad (27)$$

and perform the residual update

$$\bar{V}_t^a = V_t^a + \text{Attn}_{a \rightarrow b}(Q_t^a, K_t^b, U_t^b). \quad (28)$$

The attention logits combine an analytic *pairwise feasibility* bias with a learned *unary* geometric bias:

$$\text{Attn}_{a \rightarrow b}(Q, K, U) = \text{softmax} \left( \frac{QK^\top}{\sqrt{d}} + B_{a \rightarrow b}^{\text{epi}} + b_t^a \mathbf{1}^\top + \mathbf{1}(b_t^b)^\top \right) U. \quad (29)$$

where  $b_t^v \in \mathbb{R}^{N_v}$  stacks per-patch geometric biases  $\{b_{t,i}^v\}$  and  $\mathbf{1}$  is the all-ones vector.

**Epipolar feasibility bias.**  $B_{a \rightarrow b}^{\text{epi}}(i, j)$  encodes whether two patches can correspond under the relative camera geometry induced by  $(K^a, T_t^a, K^b, T_t^b)$ . Let  $F_{a \rightarrow b}$  be the corresponding fundamental matrix. For homogeneous patch centers  $\tilde{u}_{t,i}^a$  and  $\tilde{u}_{t,j}^b$ , we compute the point-to-epipolar-line distance

$$d_{ij} = \frac{(\tilde{u}_{t,j}^{b\top} F_{a \rightarrow b} \tilde{u}_{t,i}^a)^2}{\|(F_{a \rightarrow b} \tilde{u}_{t,i}^a)_{1:2}\|_2^2 + \epsilon}, \quad B_{a \rightarrow b}^{\text{epi}}(i, j) = -\frac{d_{ij}}{\tau}, \quad (30)$$

where  $\epsilon > 0$  avoids division by zero and  $\tau$  is a temperature.

**Learned unary geometric bias.** Analytic feasibility alone does not determine which epipolar-consistent candidate is most informative for control. We therefore predict a per-patch geometric bias with a small network (Bias-MLP) from the patch-wise geometric descriptor:

$$b_{t,i}^v = \text{MLP}(G_{t,i}^v), \quad (31)$$

which captures action relevance and view-specific reliability (e.g., proximity to the EE projection and geometry-induced saliency). The broadcast form  $b_t^a \mathbf{1}^\top + \mathbf{1}(b_t^b)^\top$  lets this unary signal modulate cross-view communication without turning it into a separate pairwise matcher.

*Geometry-conditioned feature modulation and evidence set.* Geometry should influence not only which patches communicate but also how strongly their features should be emphasized for manipulation. We

therefore condition feature modulation on compact geometric codes via a FiLM-style operator:

$$\tilde{V}_t^v(i) = \gamma(C_{t,i}^v) \odot \bar{V}_t^v(i) + \beta(C_{t,i}^v), \quad v \in \{f, h\}, \quad (32)$$

where  $\gamma(\cdot)$  and  $\beta(\cdot)$  are learned functions. Finally, we form the output evidence set by concatenating the enhanced tokens from both views:

$$x_t = \text{Concat}(\tilde{V}_t^f, \tilde{V}_t^h) \in \mathbb{R}^{N \times d}. \quad (33)$$

This design preserves detailed appearance evidence (ventral stream), constrains cross-view message passing using an epipolar feasibility prior, refines it with learned unary geometric gating from the action-centric anchor (dorsal stream), and applies geometry-conditioned modulation to emphasize control-relevant cues without over-fusing viewpoint-specific information. The resulting  $x_t$  provides the memory module with a stable and information-rich evidence stream for constructing a compact decision state under long-horizon partial observability (Section 3.3).

### A.3 Memory

The memory module maps partial observations to an actionable internal state. At each timestep  $t$ , it receives the perceptual evidence set  $x_t$  (a patch-token stream from Section 3.2) and outputs a single decision state  $h_t$ , which is the *only* memory signal exposed to the policy. This interface is intentional: instead of querying an external memory bank, long-horizon context is stored, selected, and expressed through continuous, end-to-end differentiable dynamics. Our design follows a bio-inspired division of labor. A slow episodic substrate retains spatiotemporal traces with reduced interference, while a fast working state maintains the currently relevant control context; episodic information influences behavior only by being injected into the working update, and only the fused working state is emitted as  $h_t$ .

*Multimodal Fusion.* We represent each input source as a set of tokens and fuse them into a single evidence set while preserving token identity. Let  $x_t^f \in \mathbb{R}^{N_f \times d}$  and  $x_t^h \in \mathbb{R}^{N_h \times d}$  denote the visual patch tokens from the front and hand views, respectively, and let  $p_t$  and  $\varphi_t$  denote, when available, a proprioception token and a lightweight phase token. Each token receives a modality embedding, while visual tokens additionally receive a view embedding:

$$\tilde{x}_t^v = x_t^v + E_{\text{vis}}^{\text{mod}} + E_v^{\text{view}}, \quad v \in \{f, h\}, \quad (34)$$

$$\tilde{p}_t = p_t + E_{\text{prop}}^{\text{mod}}, \quad (35)$$

$$\tilde{\varphi}_t = \varphi_t + E_{\text{phase}}^{\text{mod}} + E^{\text{phase}}(\psi_t). \quad (36)$$

We then concatenate all available tokens and apply layer normalization:

$$z_t = \text{LN}\left(\text{Concat}[\bar{x}_t^f, \bar{x}_t^h, \bar{p}_t, \bar{\varphi}_t]\right) \in \mathbb{R}^{M \times d}, \quad (37)$$

where  $M$  is the total number of fused tokens at time  $t$ . This produces a unified multimodal evidence set that can be processed jointly by the downstream memory module. We also explored an optional hexagonal positional embedding for visual tokens,

$$\bar{x}_t^v = x_t^v + E_{\text{vis}}^{\text{mod}} + E_v^{\text{view}} + E^{\text{hex}}(u_t^v), \quad v \in \{f, h\}, \quad (38)$$

where  $u_t^v$  indexes the patch-center coordinates in view  $v$ . This design was motivated by grid-cell-inspired spatial coding: compared with standard square-lattice 2D positional embeddings, a hexagonal lattice has a more isotropic local neighborhood and can provide a smoother discretization of curved physical boundaries. However, in our empirical evaluation,  $E^{\text{hex}}$  did not yield a significant performance gain. Therefore, to emphasize the core architecture and avoid unnecessary complexity, all experiments in the main paper use the simplified fusion scheme without  $E^{\text{hex}}$ .

*Dynamic context modulation.* The role of Equation (7) is not merely additive conditioning, but layer-specific reinterpretation of the same multimodal evidence under a progressively refined working context. Since the projected context term  $W_c^{(\ell)} h_t^{(\ell-1)}$  is broadcast to all  $M$  tokens, token identity is preserved while the entire token set is biased toward the current working hypothesis carried by layer  $\ell-1$ . This makes the subsequent anchor formation content-adaptive across layers without requiring explicit token rewriting or recurrent token-token interaction. In other words, different layers observe the same evidence set  $z_t$ , but under different working contexts, leading to different spatial-temporal decompositions and memory updates.

*Spatial and Temporal Anchors.* The spatial-temporal anchor construction serves as the structured interface between the multimodal evidence and the downstream slot-wise memory dynamics. In Equation (8), the routing weights  $\pi_{t,a,i}^{(\ell)}$  define how the visual evidence is organized into  $A$  anchor-conditioned components. The resulting quantity  $u_{t,a}^{(\ell)}$  should therefore be understood as the anchor-level visual evidence emphasized by spatial index  $a$ , rather than as an isolated modality-specific descriptor. By attaching the shared proprioceptive and phase tokens to every anchor, each anchor is interpreted jointly through local visual evidence and global task state, yielding

a compact anchor-conditioned token set  $\tilde{z}_t^{(\ell,a)}$ . Equation (9) then expands each anchor into  $B$  temporal modes. The learned temporal query  $q_{a,b}^{(\ell)}$  performs a slot-specific readout from  $\tilde{z}_t^{(\ell,a)}$  and produces a single latent feature  $f_{t,a,b}^{(\ell)}$  for slot  $(a, b)$ . Thus, before entering the state-space dynamics, the evidence relevant to anchor  $a$  and temporal mode  $b$  is already condensed into a slot-level latent state. This is a key distinction of our design: the model does not feed the full token collection directly into a monolithic recurrent memory, but instead first reorganizes the evidence into an  $A \times B$  matrix of compact spatiotemporal slot latents. The spatial index  $a$  determines which component of the visual evidence is emphasized, while the temporal index  $b$  determines which characteristic memory timescale is used to process that evidence. As a result, the slot matrix  $\{f_{t,a,b}^{(\ell)}\}$  provides an explicit factorization of memory addressing along both space and time.

*Selective state-space parameterization and temporal adaptation.* Given slot feature  $f_{t,a,b}^{(\ell)}$ , the projection  $\text{Proj}_{a,b}^{(\ell)}$  produces the content-dependent parameters that govern the episodic state-space update in Equation (10). As in selective state-space models, these parameters include input- and readout-dependent factors together with a step-size term, so that the effective dynamics of each slot depend on both its current content and its temporal identity. Accordingly, our temporal organization is not a naive replication of identical SSMS across the  $A \times B$  slots.

A subset of temporal slots is initialized with predefined base step sizes  $\Delta t_b^{(0)}$  spanning short to long half-lives, providing an explicit multi-timescale prior. For these prior-guided slots, the effective step size is further modulated by the slot content, so the dynamics can still contract or expand around the nominal half-life implied by  $\Delta t_b^{(0)}$ . The remaining slots do not receive such predefined temporal anchors, and instead learn their effective timescales more freely through the data-dependent parameterization produced by  $\text{Proj}_{a,b}^{(\ell)}$ . The temporal axis of the slot matrix therefore combines interpretable half-life-guided modes with more flexible learned modes, yielding a structured yet adaptive memory hierarchy rather than a bank of identical recurrent channels that differ only through input gating. For efficiency, we implement the slot-wise state-space recursion with a dedicated fused scan kernel that updates all  $A \times B$  episodic states in a single pass. This allows the model to retain explicit spatial-temporal slot structure without requiring a separate sequential scan for each slot.

*Episodic memory as latent slot-indexed engrams.* The episodic state update in Equation (11) is applied independently to each slot  $(a, b)$ , producing a bank of latent states  $\{m_{t,a,b}^{(\ell)}\}$ . These states act as hidden engrams indexed jointly by spatial component and temporal mode: spatial index  $a$  determines which anchor-conditioned evidence is stored, while temporal index  $b$  determines the characteristic retention dynamics under which it evolves. The readout  $r_{t,a,b}^{(\ell)}$  exposes only a projected expression of each engram, rather than the state itself. Hence, the memory remains structurally organized but operationally implicit: information is written into the engram through the selective state-space recursion, persists there under slot-specific dynamics, and becomes behaviorally relevant only after readout and aggregation.

This slot-indexed episodic organization is another distinctive property of our architecture. Rather than maintaining a single undifferentiated hidden state, or relying on explicit key-value retrieval over an external memory store, our model maintains a structured internal memory bank whose indices are built directly from anchor-conditioned perceptual evidence and temporal mode. This yields a notion of pattern separation inside the recurrent memory itself: different spatial-temporal components are assigned to distinct latent trajectories before recall is formed.

*Working-state integration and asymmetric memory exposure.* The episodic recall vector in Equation (12) aggregates the slot readouts into a working-space representation, which is then injected into Working Memory through Equation (13). The asymmetry between Episodic Memory and Working Memory is deliberate. Episodic states are slot-indexed, persistent, and latent; Working Memory is compact, exposed, and serves as the only inter-layer communication channel. Thus, the model separates storage from exposure: rich memory traces are preserved in the episodic bank, but only a compressed working summary is propagated upward. This differs from standard recurrent designs in which the same state must simultaneously store long-horizon information, support immediate computation, and act as the layer output.

Because Working Memory receives episodic recall only after slot-level organization and aggregation, it operates as a dynamic interpretive state rather than a raw storage tensor. The resulting  $h_t^{(\ell)}$  summarizes what the layer currently “believes” is task-relevant after querying its structured episodic bank. This design is especially important for compositional manipulation, where multiple partial cues may need to be stored on different timescales but only a small

subset should influence the next decision.

*Working readout and hierarchical memory fusion.* Equation (14) performs task-conditioned fusion over the layer-wise working readouts. Since each layer receives a different contextualized evidence set and maintains its own episodic-working interaction pattern, the readout  $y_t^{(\ell)}$  from layer  $\ell$  captures a distinct level of abstraction and temporal integration. The hierarchical fusion therefore does not simply average layers. Instead, the task query  $q_{\text{task}}$  selects which working summaries are most relevant for downstream control at time  $t$ . Lower layers may emphasize short-horizon sensory contingencies, while deeper layers may emphasize longer-horizon abstract recall. The learned layer keys  $k_{t,\ell}$  and values  $v_{t,\ell}$  allow the final memory readout  $h_t$  to adaptively combine these complementary views.

This hierarchical fusion is crucial because the memory architecture is deliberately over-complete in both space and time. The final policy does not act on the full slot bank, nor on a fixed single-layer state. Rather, it acts on a task-conditioned mixture of working summaries extracted from multiple depths of the memory hierarchy. In this sense, the final readout  $h_t$  is the output of two nested selection processes. First, evidence is factorized into slot-wise episodic traces through the anchor construction and slot-specific dynamics. Second, layer-wise working summaries are selected and fused according to task relevance. This two-stage organization, namely slot-level factorization followed by hierarchical working fusion, is what differentiates our memory from conventional recurrent backbones and enables structured long-horizon recall without explicit retrieval gates.

*HoloHead.* HoloHead regularizes the memory state  $h_t$  via a latent imagination objective: conditioned on  $h_t$ , it predicts an ordered set of  $N_a + N_c$  future waypoints in both 2D (front-camera image-plane EE projection) and 3D (normalized world-frame EE position). We decompose the rollout into a short-horizon Anchor segment and a long-horizon Compass segment,

$$\hat{W}_{t,A}^{2D}, \hat{W}_{t,C}^{2D}, \hat{W}_{t,A}^{3D}, \hat{W}_{t,C}^{3D} = \text{HoloHead}(h_t), \quad (39)$$

where  $\hat{W}_{t,A}^{\xi} = \{\hat{w}_{t+\Delta_i^{(a)}}^{\xi}\}_{i=1}^{N_a}$  and  $\hat{W}_{t,C}^{\xi} = \{\hat{w}_{t+\Delta_j^{(c)}}^{\xi}\}_{j=1}^{N_c}$  for  $\xi \in \{2D, 3D\}$ . The Anchor waypoints use the next  $N_a$  consecutive frames,

$$\Delta_i^{(a)} = i, \quad i = 1, \dots, N_a, \quad (40)$$

while the Compass waypoints are sampled non-uniformly over the remainder of the current phase.

Let  $t_{\text{end}}$  denote the end of the current phase and let  $R_t = t_{\text{end}} - t$  be the number of remaining frames. When  $R_t > N_a$ , we use logarithmic spacing from  $N_a + 1$  to  $R_t$ ,

$$\alpha_j = \frac{j-1}{N_c-1}, \quad (41)$$

$$\Delta_j^{(c)} = \lfloor (N_a + 1)^{1-\alpha_j} R_t^{\alpha_j} \rfloor, \quad j = 1, \dots, N_c.$$

and set the final Compass waypoint to the phase endpoint, i.e.,  $\Delta_{N_c}^{(c)} = R_t$ . Thus, Compass targets are sampled from near to far in a dense-to-sparse manner. When  $R_t \leq N_a$ , all Compass targets collapse to the phase endpoint.

We supervise HoloHead with

$$\mathcal{L}_{\text{holo}} = \sum_{\xi \in \{2\text{D}, 3\text{D}\}} \left( \|\hat{W}_{t,A}^\xi - W_{t,A}^\xi\|_1 + \|\hat{W}_{t,C}^\xi - W_{t,C}^\xi\|_1 \right). \quad (42)$$

Architecturally, HoloHead is a lightweight shared-trunk, dual-branch predictor. A shared MLP trunk first maps  $h_t$  to a geometric latent, which is then decoded by one branch into normalized 3D waypoints and by another branch into normalized 2D waypoints. The shared latent is also projected to a compact geometric feature for fusion with the policy stream. This objective pressures the memory dynamics to reconstruct coherent future motion from partial cues, encouraging  $h_t$  to encode both short-term actionable geometry and longer-horizon phase-level intent.

## A.4 Policy

*Single-state conditioning in implementation.* As stated in Section 3.4, the policy conditions only on the Memory Readout  $h_t$ . In implementation, we first project  $h_t$  to the policy hidden dimension:

$$c_t = W_{\text{ctx}} h_t \in \mathbb{R}^{d_{\text{pol}}}, \quad (43)$$

where  $W_{\text{ctx}}$  is a learned linear projection and  $d_{\text{pol}}$  denotes the hidden width of the policy network. This vector is used as a single conditioning token for the trajectory generator and is the only memory signal exposed to the policy.

*Trajectory tokenization.* Given the interpolated trajectory  $x_\tau \in \mathbb{R}^{H \times d_{\text{raw}}}$  from Equation (17), we embed each future end-effector pose independently into the policy hidden space:

$$z_\tau^{(0)} = W_{\text{in}} x_\tau + P \in \mathbb{R}^{H \times d_{\text{pol}}}, \quad (44)$$

where  $W_{\text{in}}$  is a learned linear projection applied to each trajectory step, and  $P \in \mathbb{R}^{H \times d_{\text{pol}}}$  is a learnable positional embedding over the prediction horizon. The policy therefore operates on the full future trajectory as a sequence of pose tokens, rather than predicting each step independently.

*Flow-time embedding.* The flow time  $\tau \in [0, 1]$  is encoded using a sinusoidal embedding followed by a two-layer MLP:

$$e_\tau = \text{MLP}(\text{PE}(\tau)) \in \mathbb{R}^{d_{\text{pol}}}, \quad (45)$$

where  $\text{PE}(\tau)$  denotes the sinusoidal time embedding. This embedding serves as the global conditioning signal for all policy blocks.

*Transformer velocity network.* The velocity network  $v_\theta$  is implemented as a stack of Transformer blocks. Let  $z_\tau^{(\ell-1)} \in \mathbb{R}^{H \times d_{\text{pol}}}$  denote the input trajectory tokens to block  $\ell$ . Each block contains three sublayers: self-attention over the trajectory tokens, cross-attention from the trajectory tokens to the single conditioning token  $c_t$ , and a feed-forward network:

$$z_\tau^{(\ell)} = \text{Block}^{(\ell)} \left( z_\tau^{(\ell-1)}; e_\tau, c_t \right). \quad (46)$$

Operationally, self-attention captures dependencies across future steps within the trajectory, while cross-attention injects the memory-conditioned decision context derived from  $h_t$ .

To make the denoising dynamics explicitly time-dependent, we modulate every block with adaptive layer normalization (AdaLN) driven by  $e_\tau$ . Concretely, the time embedding predicts per-block affine modulation and residual gating parameters for the self-attention, cross-attention, and feed-forward branches. Thus, the policy remains single-state conditioned at the interface level, while internally performing flow-time-dependent sequence reasoning over the future trajectory.

*Output parameterization.* After the final block, a modulated normalization layer and linear projection map the hidden sequence back to the raw trajectory space:

$$\hat{u}_\tau = v_\theta(x_\tau, \tau, c_t) \in \mathbb{R}^{H \times d_{\text{raw}}}. \quad (47)$$

The network therefore predicts one velocity vector for each future step and each pose dimension, matching the shape of the target velocity  $u_\tau = x_1 - x_0$  in Equation (17).

*Architecture and initialization details.* In all experiments, the policy uses 6 Transformer blocks with hidden width  $d_{\text{pol}} = 384$  and 8 attention heads. We apply dropout after input embedding and within the feed-forward sublayers. The trajectory positional embedding is initialized with a small Gaussian distribution, and linear layers are initialized with Xavier initialization. Following DiT-style practice, the final linear layers that predict AdaLN modulation parameters are zero-initialized, which makes the network start close to an unmodulated backbone and improves training stability for rectified flow matching.

*Inference.* At test time, we sample an initial trajectory  $x_0 \sim \mathcal{N}(0, I)$  and solve the ODE

$$\dot{x} = v_{\theta}(x, \tau, c_t) \quad (48)$$

with a fixed-step solver using 50 integration steps to obtain  $\hat{x}_{t:t+H}$ . Since the policy conditions only on the projected Memory Readout  $c_t = W_{\text{ctx}}h_t$ , the quality of the generated trajectory directly reflects whether the memory module has preserved the task-relevant information needed for future control.

## B Additional Experimental Details

### B.1 Camo-Dataset Statistics

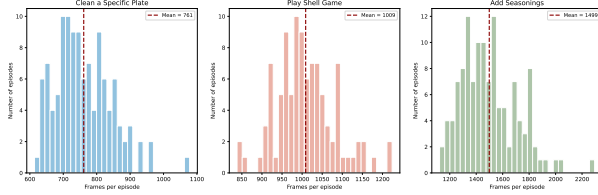


**Figure 8** Distribution of episode lengths (measured in frames) for the three tasks in Camo-Dataset: *Clean a Specific Plate*, *Play Shell Game*, and *Add Seasonings*. Each histogram shows the number of episodes falling within different frame ranges. The dashed vertical line indicates the mean episode length for each task (761, 1009, and 1499 frames, respectively).

Figure 8 shows the distribution of episode lengths in Camo-Dataset for the three tasks. Frames are recorded at 30 FPS. During training, trajectories are temporally downsampled by a factor of 4 across all tasks to reduce the effective sequence length and improve training efficiency.

### B.2 Implementation Details

*Perception.* At each timestep, the agent receives two RGB observations, one from a fixed front camera and one from a hand-mounted camera, both resized to  $224 \times 224$ . For each view, we extract patch-level appearance tokens with a frozen DINO encoder using a patch size of 14, yielding  $N_f = N_h = 256$  visual tokens of dimension  $d = 768$ . Cross-view enhancement is implemented with geometry-biased bidirectional cross-attention using 8 attention heads. As described in Section 3.2, the attention logits are biased by the end-effector anchored geometric descriptors and the analytic epipolar feasibility term, so cross-view communication is restricted to geometry-consistent and action-relevant patches. After residual cross-view enhancement and geometry-conditioned modulation, the two view-specific token sets are concatenated to form the Perception output

$$x_t = \text{Concat}(\tilde{V}_t^f, \tilde{V}_t^h) \in \mathbb{R}^{N \times d}, \quad N = N_f + N_h = 512.$$

*Memory.* Memory takes the Perception evidence  $x_t$  together with the proprioceptive state  $s_t$  and, when available, the phase signal  $\psi_t$ . A proprioception token and an optional phase token are appended to the visual evidence, and all tokens are tagged with learned modality and view embeddings as in Equation (5). The resulting fused token set is

$$z_t \in \mathbb{R}^{M \times d},$$

with  $M = N + 1$  when the phase token is absent and  $M = N + 2$  otherwise. We use  $L = 2$  memory layers and a working-state dimension  $d_w = 512$ . Each layer performs dynamic context modulation using Equation (7), decomposes the current evidence into  $A = 8$  spatial anchors and  $B = 4$  temporal anchors, and therefore maintains an  $A \times B = 32$  slot memory structure. The episodic stream is implemented with a selective state-space block using  $(d_{\text{state}}, d_{\text{conv}}, \text{expand}) = (128, 4, 1)$ , while the working stream uses  $(32, 4, 2)$ . Following Equation (10), temporal slots are associated with distinct base step sizes  $\Delta t_b^{(0)}$  and further modulated by slot content, yielding a structured multi-timescale memory. For computational efficiency, the slot-wise episodic recursion is implemented with a fused single-pass scan kernel that updates all  $A \times B$  episodic states jointly within each layer.

*Policy and HoloHead supervision.* Policy conditions only on the Memory Readout  $h_t$  and predicts a future end-effector trajectory over horizon  $H = 8$  using conditional rectified flow matching. The policy backbone uses 6 layers, hidden width 384, and 8 attention heads. During training, we sample interpolation times uniformly on  $[0, 1]$  as in Equation (17); at test time, trajectories are generated by solving the learned rectified-flow ODE with 50 integration steps. We further regularize the Memory Readout with HoloHead, implemented as a 3-layer MLP with hidden width 512. Conditioned on  $h_t$ , HoloHead predicts both 2D image-plane waypoints and 3D world-frame waypoints. The head outputs  $N_a = 8$  short-horizon Anchor waypoints and  $N_c = 8$  long-horizon Compass waypoints, matching the supervision described in Equation (15) and Equation (16).

*Optimization and sequence training.* We train the model with AdamW using a learning rate  $1 \times 10^{-4}$  and weight decay  $1 \times 10^{-6}$ . The batch size is 4. We use 100 warmup steps followed by cosine learning-rate decay, and clip gradients at a global norm of 100. Training is performed in bfloat16 with exponential moving average weights of decay 0.999. To support long-horizon sequence training, we use sequence chunks of length 512 with temporal stride 4, and apply the policy loss to the last 16 frames of each chunk. The HoloHead rollout losses use weights 0.5 for the 2D term and 0.5 for the 3D term.

**Table 3** Implementation details and hyperparameters of Chameleon, aligned with the notation in Section 3.

| Module                                 | Parameter   | Value  |
|--|---|--|
| <b>Perception</b> $\Phi_{\text{perc}}$ | Camera views  | Front RGB + hand-mounted RGB                                       |
|  | Input image resolution                                    | $224 \times 224$   |
|  | Ventral encoder   | Frozen DINOv2  |
|  | Patch size  | 14   |
|  | Patch tokens per view $(N_f, N_h)$                        | $(256, 256)$   |
|  | Token width $d$   | 768  |
|  | Cross-view enhancement                                    | Geometry-biased bidirectional cross-attention                      |
|  | Cross-view attention heads                                | 8  |
|  | Geometry terms  | EE-anchored unary patch bias + epipolar bias                       |
| Perception output $x_t$                | $x_t \in \mathbb{R}^{N \times d}$ , $N = N_f + N_h = 512$ |  |
| <b>Memory</b> $\Phi_{\text{mem}}$      | Memory input tokens $z_t$                                 | $z_t \in \mathbb{R}^{M \times d}$ , $M = N + 1$ or $N + 2$         |
|  | Working-state dimension $d_w$                             | 512  |
|  | Number of memory layers $L$                               | 2  |
|  | Spatial anchors $A$                                       | 8  |
|  | Temporal anchors $B$                                      | 4  |
|  | Total memory slots $A \times B$                           | 32   |
|  | Base temporal priors $\Delta t_b^{(0)}$                   | {0.001, 0.005, 0.02, flexible}                                     |
|  | Episodic Memory SSM                                       | $(d_{\text{state}}, d_{\text{conv}}, \text{expand}) = (128, 4, 1)$ |
|  | Working Memory SSM  | $(d_{\text{state}}, d_{\text{conv}}, \text{expand}) = (32, 4, 2)$  |
| Slot-wise state update                 | Fused single-pass scan kernel                             |  |
| <b>Policy</b> $\Phi_{\text{pol}}$      | Policy backbone depth                                     | 6 layers   |
|  | Policy width  | 384  |
|  | Policy attention heads                                    | 8  |
|  | Prediction horizon $H$                                    | 8  |
|  | Training objective  | Conditional rectified flow matching                                |
|  | Time sampling $\tau$                                      | Uniform on $[0, 1]$  |
|  | ODE solver steps (test time)                              | 50   |
| <b>HoloHead</b>                        | Head architecture   | 3-layer MLP  |
|  | Hidden width  | 512  |
|  | Anchor waypoint count $N_a$                               | 8  |
|  | Compass waypoint count $N_c$                              | 8  |
|  | Prediction spaces   | 2D image plane + 3D world frame                                    |
| <b>Optimization</b>                    | Optimizer   | AdamW  |
|  | Learning rate   | $1 \times 10^{-4}$   |
|  | Weight decay  | $1 \times 10^{-6}$   |
|  | Batch size  | 4  |
|  | Warmup steps  | 100  |
|  | Learning-rate schedule                                    | Cosine decay   |
|  | Gradient clipping   | 100  |
|  | Training precision  | bfloat16   |
| EMA decay                              | 0.999   |  |
| <b>Sequence training</b>               | Sequence chunk length                                     | 512  |
|  | Temporal stride   | 4  |
|  | Policy loss window  | Last 16 frames   |
|  | HoloHead loss weight (2D)                                 | 0.5  |
|  | HoloHead loss weight (3D)                                 | 0.5  |

### B.3 Model Size and Computational Cost of Experiment

Table 4 summarizes the parameter counts of the baseline compared. For baseline methods, we follow the parameter settings of original implementations without modification. In Chameleon, the visual encoder (DINOv2) is kept frozen and therefore does not contribute to trainable parameters. The learnable components consist mainly of geometry-based perception fusion, a hierarchical memory stack, and a flow-matching policy head. As a result, the trainable parameter count of Chameleon remains comparable

to that of existing visuomotor policies while introducing an additional memory structure.

Table 5 lists the architecture variants used in the ablation study. Each variant modifies a single component of Chameleon while keeping the remaining modules unchanged. All policies use Conditional Flow Matching (CFM). Specifically, “w/o Memory” removes the memory module, “Memory Bank” replaces the hierarchical memory with a simple memory bank, and “Vanilla Mamba” substitutes it with a standard Mamba sequence model. “w/o Dorsal Stream” removes the dorsal perception pathway, while “w/o

**Table 4** Model Complexity and Parameter Counts.

| Model  | Backbone / Components           | Trainable Parameters (M) |
|--|---------------------------------|--------------------------|
| Diffusion Policy <a href="#">Chi et al. (2023)</a>     | ResNet-18 + UNet Diffusion Head | $\approx 328.83$         |
| Flow Matching <a href="#">Zhang and Gienger (2024)</a> | ResNet-18 + UNet Velocity Net   | $\approx 79.90$          |
| ACT <a href="#">Zhao et al. (2023)</a>                 | Transformer Encoder-Decoder     | $\approx 78.13$          |
| <b>Chameleon (Ours)</b>                                | Perception + Memory + Policy    | $\approx 49.89$          |

HoloHead” removes the HoloHead training objective.

## B.4 Evaluation Metrics Definitions

*Evaluation Metrics.* Beyond the overall SR, we report three additional metrics: DSR, MSR, and CSR. MSR measures whether the robot completes the manipulation phase of a task. DSR evaluates whether the robot makes the correct decision depending on memory. To isolate decision correctness from manipulation failures, DSR is computed only over trials where manipulation succeeds:  $DSR = \frac{\text{Number of decision-success trials}}{\text{Number of manipulation-success trials}}$ . CSR evaluates the informativeness of the decision state  $h_t$ . Specifically, we roll out from  $h_t$  to predict task-relevant latent variables (e.g., the correct target object or task stage), and compute the corresponding success rate. Because decision outcomes may have non-trivial chance-level performance  $p_e$ , we additionally report the chance-adjusted *Cohen’s kappa coefficient* [Cohen \(1960\)](#) for DSR.

*Clean a specified plate.* The robot must place a cube (representing a cleaning tool) onto the contaminated plate specified by the user. After receiving the manipulation-phase instruction, the robot picks up the cube, places it on one of three candidate plates, and returns to the initial position. Evaluation protocols and chance-level statistics are summarized in Table 6. CSR is computed by rolling out the decision state  $h_t$  to predict the target plate identity.

*Play shell game.* The robot observes a human hiding a cube under one of several cups and shuffling them, and must track the hidden object before lifting the correct cup. Task definitions and success criteria follow Table 6. CSR is evaluated by predicting the correct cup from the decision state  $h_t$ .

*Add various seasonings.* The robot sequentially picks up, moves, and returns three colored seasoning spoons. Each seasoning operation consists of decision, manipulation, and recovery phases, and the full task contains nine phases in total. The phase instruction is shared by the manipulation and recovery stages to avoid information leakage. Success definitions and

chance-level statistics are summarized in Table 6. CSR evaluates whether  $h_t$  can correctly predict the current task phase.

## B.5 Failure Case Analysis

*Chameleon.* Despite strong improvements in memory-dependent decision making, Chameleon still exhibits occasional failures. As shown in Table 2, DSR and CSR across the three tasks are 100%/100%, 73.5%/91.7%, and 72.2%/85%, respectively, showing a consistent correlation. This indicates that decision failures mainly occur when HoloHead rollouts fail to predict the task-relevant latent state, corresponding to failures of pattern completion. These errors can be traced to ambiguities in the decision state  $h_t$ , suggesting imperfect pattern separation during memory encoding, potentially due to the relative weighting of the HoloHead rollout loss during training. Moreover, the dominant failure mode is manipulation rather than decision. The model typically identifies the correct target and approaches it successfully, but errors arise during grasping, such as exceeding motion limits or incorrect grasp orientation. These failures likely stem from imitation learning objectives, where trajectory matching can introduce stochastic deviations that become critical near contact. Since the policy conditions solely on the decision state  $h_t$ , persistent memory representations may occasionally introduce action ambiguity. However, given the competitive manipulation success on simpler tasks such as Clean a specified plate and Play shell game, and the best performance on the most challenging Add various seasonings task, action ambiguity is unlikely to be the primary limiting factor.

*Diffusion Policy, Flow Matching and ACT.* All three baselines achieve only chance-level performance in memory-dependent decision making. Despite the balanced distribution of task variants in the training data, the models tend to converge to a single dominant behavior, effectively predicting one decision category regardless of the underlying memory state. In this task, the diffusion policy does not exhibit the ability to capture a diverse distribution over decision trajectories. Instead, it collapses to a sin-

**Table 5** Architecture variants used in ablation studies.

| Variant           | Perception              | Memory Layers / Training              | Policy |
|-------------------|-------------------------|---------------------------------------|--------|
| Chameleon (Ours)  | Ventral & Dorsal Stream | Hierarchical Memory Stacks + HoloHead | CFM    |
| w/o Memory        | Ventral & Dorsal Stream | NA                                    | CFM    |
| Memory Bank       | Ventral & Dorsal Stream | Memory Bank                           | CFM    |
| Vanilla Mamba     | Ventral & Dorsal Stream | Vanilla Mamba                         | CFM    |
| w/o Dorsal Stream | Ventral Stream Only     | Hierarchical Memory Stacks + HoloHead | CFM    |
| w/o HoloHead      | Ventral & Dorsal Stream | Hierarchical Memory Stacks            | CFM    |

**Table 6** Task definitions and chance-level success rates.

| Task                    | Candidates | Manipulation Success                 | Decision Success                      | Chance-Level             |
|-------------------------|------------|--------------------------------------|---------------------------------------|--------------------------|
| Clean a specified plate | 3 plates   | Complete<br>pick-place-return        | Place the cube on<br>the target plate | DSR = 1/3,<br>CSR = 1/3  |
| Play shell game         | 3 cups     | Lift any cup                         | Lift cup containing<br>cube           | DSR = 1/3,<br>CSR = 1/3  |
| Add various seasonings  | 3 spoons   | Complete three<br>pick-season-return | Correct order:<br>green-red-yellow    | DSR = 1/27,<br>CSR = 1/9 |

gle dominant behavior. It is somewhat unexpected, as diffusion policies are known for their ability to model multimodal action distributions rather than collapsing to a single deterministic behavior. In terms of manipulation performance, the baselines achieve high success rates on simple pick-and-place tasks. However, on the more complex task, which involves longer action sequences and higher task complexity, their performance degrades substantially.

*Memory Bank and Vanilla Mamba.* In the MemoryBank variant, we replace the memory module of Chameleon with a simple memory bank that stores past latent features together with a similarity-based retrieval mechanism. The retrieved memories are directly concatenated with the current observation before being passed to the policy. We hypothesize that similarity-based retrieval is unstable under perceptual aliasing, since visually similar but decision-irrelevant past observations can be retrieved together with truly relevant ones. This introduces ambiguity into the recalled context, causing the policy to confuse relevant and irrelevant history. As a result, the policy fails to maintain a consistent behavioral strategy and often exhibits random movements near the initial position, losing the ability to complete the manipulation task.

In the Vanilla Mamba variant, the structured episodic-working memory of Chameleon is replaced by a single monolithic state-space backbone. As a result, the model lacks explicit pattern separation during memory encoding and also lacks a goal-directed recall mechanism before policy conditioning. Under perceptual aliasing, task-relevant cues are therefore mixed with irrelevant observations in a single recurrent state, making the model uncertain about what should be

preserved, prone to forgetting the weak but crucial contextual signal needed for later disambiguation, and unable to selectively expose the right memory at decision time. Empirically, this leads to unstable behavior across trials: once the latent cue is overwritten or diluted, the policy can no longer maintain a consistent memory-dependent strategy and often falls back to incorrect or near-random actions.

*w/o Dorsal Stream.* This variant exhibits the largest drop in success rate compared to Chameleon in the Play shell game task. This task involves frequent changes in spatial relations and requires the model to perform a certain degree of spatial reasoning. Consequently, this variant shows a higher tendency toward random failures. Unlike the baselines, where memory completely fails, and the policy collapses to interacting with a fixed target, this model tends to randomly interact with one of the candidate objects after failure, rather than consistently collapsing to a specific target.

*w/o HoloHead.* The model exhibits a certain degree of memory capacity. However, due to the misalignment between the open-loop training objective and the temporal locations of the memory frames, the model fails to learn stable memory utilization. As a result, the recalled context is inconsistent, and the overall memory performance remains unstable.

## C Human Episodic Memory and Correspondence to Chameleon

### C.1 Overview of the EC–HC–PFC Episodic Memory Circuit

Human episodic memory is commonly associated with the interaction between the medial temporal lobe and the frontal cortical systems. In particular, the EC, the HC, and the PFC form a functional circuit that supports the encoding, storage, and retrieval of episodic experiences. Sensory information processed across distributed cortical regions converges onto the medial temporal lobe, where the HC integrates multimodal inputs into event-specific representations. These representations can later be reactivated to reconstruct past experiences and guide behavior.

At the systems level, cortical association areas project to the HC primarily via the EC. The hippocampus binds together distributed sensory representations into coherent episodic traces and subsequently reinstates activity in neocortical regions during recall. Meanwhile, the prefrontal cortex interacts with hippocampal memory to organize encoding, control retrieval, and integrate recalled information with ongoing decision processes. This EC–HC–PFC loop, therefore, provides the neural substrate for memory-guided behavior and flexible cognition, describing how HC–neocortical connectivity enables recall by reinstating cortical activity patterns associated with stored episodes.

### C.2 Perceptual Pathways: Ventral and Dorsal Streams

Before reaching the memory system, sensory information is processed through specialized perceptual pathways in the neocortex. In the visual domain, two major streams are commonly distinguished: the ventral “what” pathway and the dorsal “where” pathway. The ventral stream projects from early visual areas toward the temporal cortex and encodes object identity and semantic features, while the dorsal stream projects toward the parietal cortex and represents spatial relationships and action-relevant geometry. These complementary streams provide the HC with both object-centered and spatial information necessary for constructing indexed episodic representations. By combining these signals, the HC can encode events as structured associations between objects, locations, and contextual cues.

Inspired by this biological organization, we design the perception module with a similar dual-stream

structure. A ventral pathway extracts patch-level appearance features from the input images, providing detailed visual evidence about what is present in the scene. In parallel, a dorsal pathway computes EE-anchored geometric descriptors that encode action-centric spatial relations, supplying the where structure relevant for manipulation. These two streams interact through geometry-grounded cross-view communication, allowing appearance evidence and spatial structure to be integrated while preserving viewpoint-specific cues. The resulting representation forms a structured evidence set that jointly captures visual appearance and control-relevant geometry and is stored in the memory module as the perceptual basis for episodic decision-making.

### C.3 Entorhinal Cortex: Interface Between Perception and Memory

Within the HC formation, the EC and DG together constitute the initial stage of HC information processing and play a central role in encoding episodic memory. The entorhinal cortex acts as the principal interface between the neocortex and the hippocampus, integrating sensory and contextual information from distributed cortical areas. Neurons in the superficial layers of the EC project to the DG through the perforant path, transmitting a highly convergent representation of the current sensory and spatial context.

While the EC provides a rich but often overlapping representation of ongoing experience, the DG transforms this input through a process commonly described as pattern separation. Granule cells in the DG receive convergent projections from large populations of EC and operate under strong inhibitory control, leading to extremely sparse neural activity. As a result, similar patterns of EC activity are mapped onto more decorrelated population codes in the DG. Through this EC–DG transformation, the hippocampal system reduces interference between similar experiences and enables the encoding of distinct episodic memories even when sensory inputs are highly similar.

The multimodal fusion and slot formation mechanism in our memory module plays a role analogous to the EC–DG transformation. The perception module first produces patch-level evidence tokens from multiple sensory sources, which correspond to the multimodal cortical inputs arriving at the EC. These tokens are then fused and decomposed into spatial anchors, forming localized summaries of the visual scene. The subsequent expansion into multiple spatiotemporal slots further decorrelates the evidence

**Table 7** Biological inspiration and correspondence to the Chameleon.

| Biological component | Biological role   | Chameleon module   | Functional correspondence  |
|----------------------|---|--|--|
| Ventral stream       | Encodes object identity information ( <i>what</i> ).  | Patch-level tokens from the frozen DINO encoder                                      | Provides detailed local visual evidence about objects, boundaries, and contact-relevant regions.   |
| Dorsal stream        | Encodes spatial relations and geometry ( <i>where</i> ).  | EE-anchored spatial geometric descriptors, and geometry-biased cross-view attention. | Supplies spatial structure, including cross-view correspondence between the front and hand cameras.  |
| EC                   | Integrates multimodal sensory/contextual inputs.  | Multimodal fusion of visual, proprioceptive, and phase tokens                        | Converts heterogeneous sensory signals into a unified evidence set that can be processed by memory.  |
| DG                   | Performs pattern separation.  | Spatial anchors and spatiotemporal slot.   | Expands overlapping perceptual evidence into structured slot representations indexed by spatial component and temporal scale.  |
| HC circuit           | Supports the encoding and retrieval of structured episodic representations.                                 | Hierarchical episodic memory stack.  | Maintains structured episodic memory across slots and time.  |
| CA3                  | Stores episodic traces and supports pattern completion.   | Slot-wise episodic state-space memory.   | Maintains distributed episodic states whose dynamics support context recovery from partial observations.   |
| CA1                  | Integrates HC recall into an output representation that can be communicated to downstream cortical systems. | Aggregated episodic recall vector and layer-level working readout.                   | Combines information recalled from multiple episodic slots into a compact representation for downstream use.   |
| HC-PFC interaction   | Supports retrieval, prospective cognition, and memory-guided decision-making.                               | Working state $h_t$ with hierarchical fusion.  | Aggregates recalled episodic content into a compact decision-oriented state analogous to prefrontal working representations.   |
| PFC imagination      | Recombines retrieved episodic content to predict future states and evaluate candidate actions.              | HoloHead latent imagination module   | Performs prospective simulation by predicting multi-horizon future EE trajectories, shaping $h_t$ into a predictive representation of future motion and task progress. |

by projecting it into a higher-dimensional structured representation indexed by spatial component and temporal scale. Similar observations that differ in subtle spatial or temporal cues therefore activate different slot patterns, reducing interference between episodes. Although our model does not explicitly implement a learned pattern separation mapping as in biological EC–DG circuits, the spatial–temporal slot decomposition organizes perceptual evidence into structured components that reduce interference between similar observations. In this sense, it functions analogously to the pattern separation operation of the EC–DG pathway, transforming overlapping perceptual inputs into a representation suitable for episodic storage.

#### C.4 Hippocampus: Pattern Separation and Pattern Completion

Within the HC formation, multiple interconnected subfields cooperate to support episodic encoding and retrieval. After the EC–DG transformation produces decorrelated representations, these signals are transmitted to CA3 through the mossy fiber pathway. Unlike the sparse coding regime of DG, CA3 contains extensive recurrent collateral connections that form

an auto-associative network. These recurrent connections enable pattern completion: partial or degraded inputs can trigger attractor dynamics that reactivate the stored representation associated with the original experience. Through the complementary operations of pattern separation and pattern completion, the HC circuit can both encode distinct events and retrieve them from incomplete sensory cues. Neurophysiological studies further suggest that HC neurons integrate spatial, object-related, and contextual information into conjunctive activity patterns, effectively binding distributed cortical representations into coherent episodic memories.

The episodic state-space memory in our architecture parallels key computations of the HC circuit. Each spatial–temporal slot maintains an episodic state that evolves through a selective SSM, acting as a distributed memory trace indexed by spatial component and temporal resolution. The slot-wise SSM dynamics preserve long-lived episodic information while allowing content-dependent updates through learned input factors. When new evidence arrives, these episodic states are updated and subsequently read out through slot-specific projections, producing recall vectors that summarize relevant stored information.

This mechanism resembles HC pattern completion in that the episodic states can recover relevant past context even when the current observation provides only partial evidence. In biological systems, episodic memory is often described as a cortical storage system indexed by the HC, with CA3 attractor dynamics supporting replay-based retrieval. Our architecture does not explicitly model these mechanisms; instead, information storage and retrieval are implemented through direct differentiable information flow within the slot-wise memory dynamics. The aggregated recall vector then plays a role analogous to the CA1 output stage, integrating contributions from multiple episodic traces into a compact representation consumed by downstream modules.

a summary of experience but also a representation predictive of upcoming motion and task progress.

## C.5 Hippocampus–Prefrontal Cortex Interaction

Although the HC encodes and retrieves episodic representations, adaptive behavior requires additional mechanisms that organize memory for future-oriented decision making. A large body of evidence suggests that interactions between the HC and PFC support such prospective cognition. In particular, prefrontal circuits are believed to guide the retrieval and recombination of episodic memories to simulate possible future states and evaluate candidate actions. During goal-directed behavior, HC activity provides fragments of experience, while PFC circuits organize these fragments into structured predictions about future trajectories and task outcomes.

Our architecture mirrors this HC–PFC interaction through the coupling between episodic memory and a compact working state. While the episodic states store distributed traces of past observations, the working state  $h_t$  aggregates recalled episodic information into a representation suitable for decision making, playing a role analogous to prefrontal working representations. Conditioned on this state, the HoloHead module performs latent imagination by predicting future end-effector trajectories across multiple horizons. The short-horizon Anchor predictions capture immediate control geometry, whereas the long-horizon Compass predictions summarize the broader phase-level motion structure.

In this view, episodic memory provides contextual fragments of experience, while the working state organizes these fragments into a predictive representation of future behavior. The imagination objective implemented by HoloHead encourages  $h_t$  to encode task-relevant future structure, analogous to prospective simulation in prefrontal–hippocampal circuits. As a result, the decision state  $h_t$  becomes not only